EAI Endorsed Transactions
on AI and Robotics

Research Article EAI.EU

Review On: The Service Robot Mathematical Model

Ata Jahangir Moshayedi[1,*], Atanu Shuvam Roy[1], Sithembiso Khaya Sambo[1], Yangwan Zhong[1], Liefa Liao[1]

[1]School of Information Engineering, Jiangxi University of Science and Technology, 86 Hongqi Avenue, Ganzhou, Jiangxi, China 341000

Abstract

After nearly 30 years of development, service robot technology has made important achievements in the interdisciplinary aspects of machinery, information, materials, control, medicine, etc. These robot types have different shapes, and mainly in some are shaped based on application. Till today various structure are proposed which for the better analysis's need to have the mathematical equation that can model the structure and later the behaviour of them after implementing the controlling strategy. The current paper discusses the various shape and applications of all available service robots and briefly summarizes the research progress of key points such as robot dynamics, robot types, and different dynamic models of the differential types of service robots. The current review study can be helpful as an initial node for all researchers in this topic and help them to have the better simulation and analyses. Besides the current research shows some application that can specify the service robot model over the application.

Keywords: Service robot, AGV, Two Wheel Differential, Three Wheel, Four Wheel, Four Wheel Skid Steering, Six Wheel,

Ackermann AGV, Crawler Robot, Legged Robot, Snake Robot medical image recognition, character recognition.

Received on 28 November 2021, accepted on 12 February 2022, published on 23 February 2022

doi: 10.4108/airo.v1i.20

1. Introduction

As an inevitable extension of computer technology and modern comprehensive technology, home service robot technology known as service robots will achieve a breakthrough at an unprecedented speed. Service robots are entering various places from home to industries and are even recently accepted as home appliances. The history of robotics shows that the service robot chapter started with the Automated Guided Vehicle (AGV) [1] and then various applications bring the various shapes furnished with different structures. AGV's were initially as the load carriers but are now being used for more applications [2-3]. Then, for a better analysis of a service robot, researchers must examine mathematical modeling for a better control algorithm [4] and dynamic simulation as necessary stages in the robotic domain and studies. This equation which called Dynamic modelling involves deriving equations that clearly describe the relationship between forces and motions in a system. The paper's main aim is to describe the different types of service robot models, especially the Automated Guided Vehicle (AGV), showcase work related to the individual types, and state their proposed dynamic models. This paper is set as follows initially, the service robot overview is discussed, then based on the different structures of service robots, review the different kinematic and dynamic models described. Finally, the comparison between the shapes and application are discussed at the end.

2. Service Robot Models

Currently, Service Robots are an umbrella term for various types of robots and consider as any type of robot that can give the service or in place of a human. One of the most famous groups of service robots, which initially started from industry but are now used as a part of home applications, are Automated Guided Vehicle (AGV). Initially, AGV was known as a complex machine representing a complete material handling solution, installed in many industries and widely used to efficiently

* Corresponding author. Email: aminkolahdooz@gmail.com

transport materials through a facility [5]. AGV can increase efficiency and productivity and reduce product damage and labour costs. The overall view of service robots shows that usually, a mobile robot has two subsystems, Drive Subsystem and Mechanical Subsystem, as shown in figure 1.

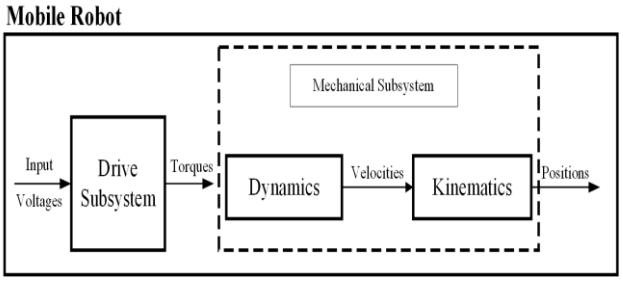

Figure 1. An electrical robot's decomposition

As it is shown in figure 1, the Drive subsystem takes in voltages and controls the motor functions. The mechanical subsystem has dynamics and kinematics, which require various algorithms and has models that help determine steering or tracking of paths, i.e., positioning or orientation of the robot. Understanding the mathematical equation and relation between each part will help for better control and design of the robot. The reported shape and structure of Service robots can be named as Two Wheel Differential, three-wheel, four-wheel AGV, Four Wheel Skid Steering AGVs, Six Wheel AGVs, Ackerman AGV, crawler and legged robot as described in the following;

2.1 Two Wheel Differential

The differential drive is a two-wheel drive system with independent actuators for each wheel. The name refers to that the robot's motion vector is the sum of independent wheel motions. The robot's driving wheels are normally mounted on both sides, facing forward. [6]. Pure tracking in this type of robot is at least as good as the others and is easier to implement and understand [7]. Considering the mathematical equation, the different variables of the two-wheel differential robot are shown in Figure (2).

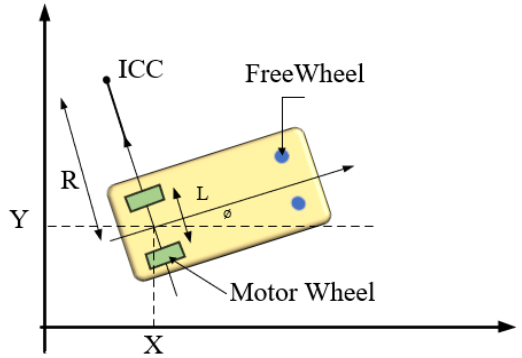

Figure 2. Two Wheel Differential Robot Schematic.

As it is shown in Figure 2, The ICC, which stands for instantaneous centre of curvature, and the front of the robot have two freewheels, as shown in figure (2), with L being the difference between the two back motor wheels. ϕ is the angle at which the robot is turned from the centerline to the x-axis. R is the distance from ICC to the midpoint between the two back wheels. Considering the above variables, to follow the robot and find the robot velocity. The inputs required for the motion of a mobile robot are the linear velocity (V) and orientation [8-9]. The rate of change of position of robot along the x-direction is $\dot{x}$ and that in the y-direction is $\dot{y}$ are stated by

$$\dot{x} = V\cos(\theta)$$
$$\dot{y} = V\sin(\theta) \quad (1)$$

and the angular velocity of the robot is given by

$$\dot{\theta} = \omega = \frac{(V_r - V_l)}{L} \quad (2)$$

Substituting the linear velocity V.

$$\dot{x} = \frac{(V_l + V_r)}{2}\cos(\theta)$$
$$\dot{y} = \frac{(V_l + V_r)}{2}\sin(\theta) \quad (3)$$

The velocity V of the robot in a fixed reference coordinate system is therefore given by

$$V = \sqrt{\dot{x}^2 + \dot{y}^2} \quad (4)$$

$$V = \sqrt{\left(\frac{(V_l + V_r)}{2}\cos(\theta)\right) + \left(\frac{(V_l + V_r)}{2}\sin(\theta)\right)} = \frac{V_r + V_l}{2} \quad (5)$$

The individual velocities, Vr and Vl, can now be calculated using the equations:

$$V_r = \left(V + \frac{L}{2}\omega\right)$$
$$V_l = \left(V - \frac{L}{2}\omega\right) \quad (6)$$

The outputs, V_r and V_l then used to generate the output $\dot{x}$, $\dot{y}$ and ω using the above equations [10-13]

The following equations (7) are the forward kinematic mathematical equations stated by the researchers, which in them the Angular momentum of the robot presented

$$\omega(R + 1/2) = v_r$$
$$\omega(R - 1/2) = v_l \quad (7)$$

V_r is the velocity of the right wheel while $v_l$is the velocity of the left wheel, then from (7): the value (R distance from ICC) and (ω Angular momentum) defined as shown in equation (7)

$$R = 1/2 \star (v_l + v_r)/(v_r - v_l) \quad (8)$$
$$\omega = (v_r - v_l)/1$$

The forward kinematics equation (9) (concerning time):

$$dx/dt = m(t)\cos(\theta(t)) \quad (9)$$
$$dy/dt = m(t)\sin(\theta(t))$$

Then the change of direction with respect to time is the same as the angular rate ω. Therefore,

$$d\theta/dt = \omega = (v_r - v_1)/1 \quad (10)$$

Integrating the equation(4) gives a function for the robot's orientation with respect to time. The robot initial orientation θ(0) is also replaced by θ_0:

$$\theta(t) = (v_r - v_1)t/1 + \theta_0$$
$$dx/dt = [(v_r + v_1)/2]\cos(\theta(t)) \quad (11)$$
$$dy/dt = [(v_r + v_1)/2]\sin(\theta(t))$$

Taking the initial positions to be x(0) = x0, and y(0) = y0 to get:

$$x(t) = \quad (12)$$
$$x_0 + 1/2(v_r + v_1)/(v_r - v_1)$$
$$[\sin((v_r - v_1)t/1 + \theta_0) - \sin(\theta_0)]$$
$$y(t) =$$
$$y_0 - 1/2(v_r + v_1)/(v_r - v_1)$$
$$[\cos((v_r - v_1)t/1 + \theta_0) - \cos(\theta_0)]$$

As $\frac{1/2(v_r + vl)}{(v_r - vl)} = R$, the robots turn radius, and $\frac{(v_r - vl)}{l} = \omega$, The above equations can be reduced to :

$$x(t) = x_0 + R[\sin(\omega t + \theta_0) - \sin(\theta_0)] \quad (13)$$
$$y(t) = y_0 - R[\cos(\omega t + \theta_0) - \cos(\theta_0)]$$

Substituting the terms v_r and v_l With sr and sl, which indicates displacements instead of speeds, allows dropping the time variable t . Here s_r and s_1 do the left and right wheels travel the distances respectively. Finally, the equation becomes:

$$\&x(t) = x_0 + 1/2(s_r + s_1)$$
$$/(s_r - s_1)[\sin((s_r - s_1)/1 + \theta_0) - \sin(\theta_0)]\&$$
$$y(t) = y_0 - 1/2(s_r + s_1)$$
$$/(s_r - s_1)[\cos((s_r - s_1)/1 + \theta_0) - \cos(\theta_0)] \quad (14)$$

Another mathematical model with the aim of showing in the kinematic equations relating to differential drive robots are discussed and implemented by [14]. For autonomous navigation of the robot, it must always know its position, i.e. the translation matrix and the rotation matrix. When the robot speed of the wheel change, the robot has to rotate around a point on the common axis of the two driving wheels, called the Instantaneous Centre of Curvature (ICC). Suppose the robot is at some location (x, y), making an angle of θ with the X axis. After some time, the robot's position will shift, and a new one will be (x', y') and the new angle is θ'.

$$ICC = [x - R\sin(\theta), y + R\cos(\theta)] \quad (15)$$

and at time $t + \delta t$ the new positions would be:

$$\begin{pmatrix} x' \\ y' \\ \theta' \end{pmatrix} = \begin{pmatrix} \cos(\omega\delta t) & -\sin(\omega\delta t) & 0 \\ \sin(\omega\delta t) & \cos(\omega\delta t) & 0 \\ 0 & 0 & 1 \end{pmatrix} \begin{pmatrix} x - ICC_x \\ y - ICC_y \\ \theta \end{pmatrix} + \begin{pmatrix} ICC_x \\ ICC_y \\ \omega\delta t \end{pmatrix} \quad (16)$$

by using equation (16), the user can find the robot's position at any instant. The above equations can be described as the position of the robot moving in a particular direction θ_t at a given velocity V (where V is the average of the left wheel and the right wheel velocity) by:

$$P_x = x_t = \int V \cdot \sin\theta \cdot d\theta$$
$$P_y = y_t = \int V \cdot \cos\theta \cdot d\theta \quad (17)$$
$$\theta = \int \omega \cdot dt$$

The dynamic model of Two Wheel Differential robot (Khepera IV) [15]is derived from the kinematic and dynamic relations as follows:

$$F_L + F_R = m \cdot a$$
$$\frac{(F_R - F_L)D}{2} = J \cdot \varepsilon \quad (18)$$

Where the dynamic parameters of the robot are, F_L and F_R = Applied forces to the left and right wheels, respectively. m as Mass of the robot,a tangential acceleration, J moment of inertia and ε angular acceleration. The following are the model's inputs, outputs, and state variables:

$$x(t) = [x_1(t), x_2(t), x_3(t), x_4(t)]$$
$$= [v(t), \omega(t), \omega_L(t), \omega_R(t)]$$
$$u(t) = [u_1(t), u_2(t), u_3(t), u_4(t)] = [F_L, F_R, U_L, U_R] \quad (19)$$
$$y(t) = [y_1(t), y_2(t)] =$$
$$[x_3(t), x_4(t)] = [\omega_L(t), \omega_R(t)]$$

Where $U_L$and U_R are the voltages applied to the DC motors that drive the robot's wheels,

$$x_1(t) = v(t) \quad (20)$$

We have after deriving from the sides of the equation $\dot{x}_1(t) = a(t)$ and using equation (29) the following relation will be obtained:

$$\dot{x}_1(t) = \frac{F_L + F_R}{m} = \frac{1}{m}F_L + \frac{1}{m}F_R \quad (21)$$

From equation (29), $u_1(t) = F_L$ and $u_2(t) = F_R$. As a result, equation (13) can be written as follows:

$$\dot{x}_1(t) = \frac{1}{m}u_1(t) + \frac{1}{m}u_2(t) \quad (22)$$

With this equation $x_2(t) = \omega(t)$ we can get a deduction from the equation $\dot{x}_2(t) = \varepsilon(t)$. The second state equation is given by applying equation (9):

$$\dot{x}_2(t) = \frac{-D}{2J}u_1(t) + \frac{D}{2J}u_2(t) \tag{23}$$

The angular velocities U_L and U_R were generated using ω_L and ω_R, respectively. The following equations describe the voltage values of the motors:

$$\begin{aligned} J\varepsilon_L(t) + F\omega_L(t) + F_L r = U_L \\ J\varepsilon_R(t) + F\omega_R(t) + F_R r = U_R \end{aligned} \tag{35}$$

The angular accelerations of the wheels are $\varepsilon_L$and ε_R, and the friction force is F. By opting for the third state, variable as $x_3(t) = \omega_L$ and fourth state variable as $x_4(t) = \omega_R$. The following state equations can be constructed by using $U_L$and U_R as third and fourth input variables, respectively:

$$\begin{aligned} \dot{x}_3(t) = -\frac{F}{J}x_3(t) - \frac{r}{J}u_1(t) + \frac{1}{J}u_3(t) \\ \dot{x}_4(t) = -\frac{F}{J}x_4(t) - \frac{r}{J}u_2(t) + \frac{1}{J}u_4(t) \end{aligned} \tag{36}$$

As a result, there are four state equations that can be expressed as a state-space matrix, as shown below:

$$\begin{aligned} \dot{x}(t) &= \begin{bmatrix} 0 & 0 & 0 & 0 \\ 0 & 0 & 0 & 0 \\ 0 & 0 & -\frac{F}{J} & 0 \\ 0 & 0 & 0 & -\frac{F}{J} \end{bmatrix} x(t) + \begin{bmatrix} \frac{1}{m} & \frac{1}{m} & 0 & 0 \\ -D & \frac{D}{2J} & 0 & 0 \\ -\frac{r}{J} & 0 & \frac{1}{J} & 0 \\ 0 & -\frac{r}{J} & 0 & \frac{1}{J} \end{bmatrix} u(t) \\ y(t) &= \begin{bmatrix} 0 & 0 & 1 & 0 \\ 0 & 0 & 0 & 1 \end{bmatrix} x(t) \end{aligned} \tag{37}$$

2.2 Three Wheel

The three-wheeled robots are divided into two parts, Differential steering (2 driving wheels with additional free rotating wheels to maintain body balance) and Two wheels powered by a single power source and one for the third cycle power steering. The robot's steering can be changed by changing the relative rate of rotation of the two separate drive wheels for differential steering wheels. The robot will go straight ahead if both wheels are propelled in the same direction and at the same speed. Otherwise, the centre of rotation can fall anywhere on the straight line joining the two wheels, depending on the speed and direction of rotation. [16]. Figure 3 shows the schematics of a three-wheeled robot. The back wheels represent the motor wheels, and the front is the steering wheel.

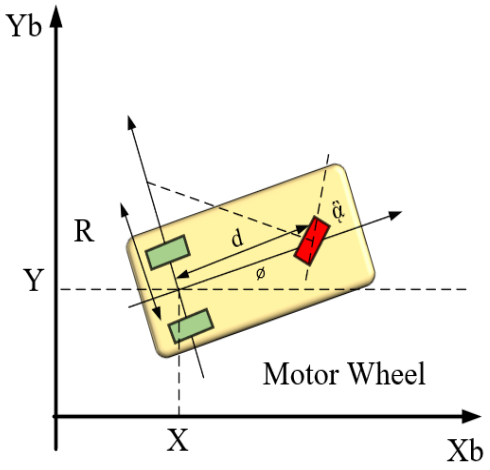

Figure 3. Three Wheel Robot Schematics.

As shown in [8] [9], the robot velocity cab be defined as (38)

$$\begin{aligned} v_x = v_u \sin\psi + v_w \cos\psi \\ v_y = v_u \cos\psi - v_w \sin\psi \end{aligned} \tag{38}$$

In (39) we observe v_x and v_y which are the lateral parts of the velocity of the AGV mass centre in the UCW frame. $\dot{\psi}$ is the position of the vehicle's steering wheel at any given time. Both UCW and XOY have an angular velocity of w = $\dot{\psi}.\delta$ is the steering angle, which is defined as the angle between the steering wheel and the vehicle's longitudinal axis cu.In the two coordinate frames, a_u , a_w, a_x and a_y are employed for acceleration components. The resultant of the forces produced by the tires on the vehicle has longitudinal (u) and lateral (w) components, as indicated. The subscripts R and L stand for Right and Left (for rear tires), respectively, while the subscripts r and f stand for rear and front, respectively. Thus, the lateral (w) components of the force (F) from the rear (r) left (L) tire are denoted as (F_{ur})L. The longitudinal components of the forces generated by the two rear tires, on the other hand, are the same and are represented by (40).

$$\begin{aligned} 2F_{ur} + F_{uf}\cos\delta - F_{wf}\sin\delta = ma_u \\ (F_{wr})_L + (F_{wr})_R + F_{wf}\cos\delta + F_{uf}\sin\delta = \mathrm{ma}_w \end{aligned} \tag{40}$$

$$-[(F_{wr})_R + (F_{wr})_L]b + (F_{wr}\cos\delta + F_{uf}\sin\delta)a = I\dot{\omega} \tag{41}$$

where a and b are the two distances from two of the wheels (one in the front centre and one from the back out of two) toward the perpendicular from the centroid of the vehicle. I is the moment of inertia about a vertical axis passing through the centre of mass, a_u and a is the $u-$ and $w-$ components of the acceleration of point c, the mass centre, and ω is the angular acceleration. It can be shown that and a can be written in the following form.

$$a_u = \dot{v}_u - v_v\omega$$
$$a_w = \dot{v}_w + v_u\omega \quad (42)$$

where v_u and v_w are the components of the velocity in the vehicles coordinate system. Then the dynamic equations of the plane motion for the vehicle are

$$m\dot{v}_u = mv_w\omega + 2F_{ur} + F_{uf}\cos\delta - F_{wf}\sin\delta$$
$$m\dot{v}_w = -mv_u\omega + (F_{wr})_L + (F_{wr})_R + F_{wf}\cos\delta + F_{uf}\sin($$
$$I\dot{\omega} = -[(F_{\omega r})_R + (F_{wr})_L]b + (F_{wr}\cos\delta + F_{uf}\sin\delta)a \quad (43)$$

The above equations have been used for the simulations carried out in this study. As it was mentioned earlier, it is assumed that the side slip angles are small, and thus, the corresponding side forces are determined from (44) and (45).

$$F_{wr} = C_f\beta_f \quad (44)$$

$$(F_{wr})_{L,R} = C_r(\beta_r)_{L,R} \quad (45)$$

where β_f, β_{rL} and β_{rR} are the slip angles for the front, rear left and rear right tires, respectively, and C_r and C_r are the cornering stiffness of the front and rear wheels, respectively. The slip angles for the front and rear tires can be determined as follows:

$$\beta_f = \delta - \tan^{-1}\frac{v_w + a\omega}{v_u} \quad (46)$$

$$(\beta_r)_R = \tan^{-1}\frac{b\omega - v_w}{v_u - d\omega}$$
$$(\beta_r)_L = \tan^{-1}\frac{b\omega - v_w}{v_u + dw} \quad (47)$$

Where 2d is the distance between the rear tires.

2.3. Four Wheel AGVs

The four-wheeled robot is the most balanced robot among other wheeled robots. Although three wheels are enough to maintain static stability, the three-wheeled robot can lose its balance while moving. Four-wheeled robots rarely lose their stability when moving. The four-wheeled robot can be controlled using differential steering and a steering method similar to a car. This model was introduced in 2 Degree of Freedom (DOF) and 7 DOF, as shown in the following.

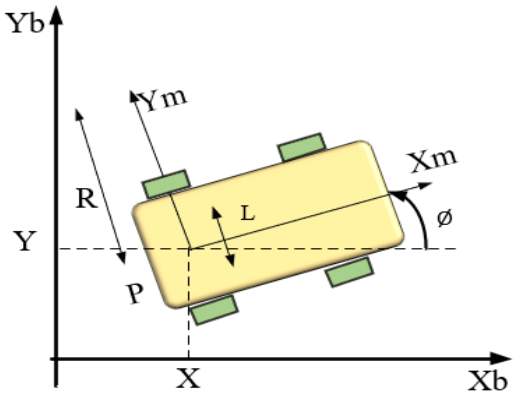

Figure 4. Four-wheel robot schematics.

The Four-Wheel AGVs model with the 2 Degree of Freedom (DOF): vehicle model is shown in equation (48) [17].

$$m(\dot{v}_y + v_x\omega) = (C_f + C_r)\beta + \frac{1}{v_y}(aC_f - bC_r)\omega - C_f\delta$$
$$I_z\dot{\omega} = (aC_f - bC_r)\beta + \frac{1}{v_x}(a^2C_f + b^2C_r)\omega - aC_f\delta \quad (49)$$

In (59), m denotes vehicle mass; C_f ,C_r cornering stiffness of the front and rear axle; a, b the distance of the centre of gravity to front and rear axle; I_z turning inertia around Z axle; V_x, V_y longitudinal and lateral velocity, ω yaw rate; δ front-wheel steering wheel; sideslip angle.

A) The Four-Wheel AGVs model with the 7 DOF Vehicle Model:
this model contains Longitudinal and Lateral movement as shown in (60), (61).

$$m(\dot{v}_x - v_y\omega) = (F_{xfr} + F_{xfr})\cos\delta - (F_{yfr} + F_{yfl})\sin\delta + F_{xrl} + F_{xrr} \quad (50)$$

$$(F_{xfr} + F_{xfl})\sin\delta + F_{yrl} + F_{yrr}$$

$$m(\dot{v}_y + v_x\omega) = (F_{yfl} + F_{yfr})\cos\delta + (F_{xfr} + F_{xfl})\sin\delta + F_{yrl} + F_{yrr} \quad (51)$$

then the Yaw movement as shown in equation (62)

$$I\dot{\omega} = a(F_{yfl} + F_{yfr})\cos\delta + \frac{d}{2}(F_{yfl} - F_{yfr})\sin\delta - b(F_{yrl} + F_{yr}) + \frac{d}{2}(F_{xfr} - F_{xfl})\cos\delta + a(F_{xfl} + \text{a}$$
$$F_{xff})\sin\delta + \frac{d}{2}(F_{xrr} - F_{xll}) \quad (52)$$

and finally, the rotation of the wheel equation (53) described the wheel rolling inertia wheel rational rate relation to wheel brake torque.

$$J_\omega\dot{\omega}_\omega = T_{dij} - T_{bij} - F_{xij}R_\omega \quad (54)$$

In (63), $F_{\mathrm{xfl}}, F_{\mathrm{xfr}}, F_{\mathrm{xrl}}, F_{\mathrm{xrr}}, F_{\mathrm{yfl}}, F_{\mathrm{yfr}}, F_{\mathrm{yrl}}, F_{\mathrm{yrr}}$ force components for front left, front right, rear left and rear right tire along x, y coordinates respectively; d distance between leaf and right wheels; J_ω wheel rolling inertia; ω_{ij} wheel rational rate; T_{bij} wheel brake torque ($i = f, r$ front, rear-wheel, $j = l, r$ left, right wheel) ; $T_{\mathrm{d}ij}$ rear wheel driving torque; $F_{\mathrm{x}ij}$ wheel longitudinal force; R_ω wheel rolling.

Another model introduced [18] is that the vehicle follows the desired velocity profile, enabling a comfortable and safe ride. Catered the lateral dynamic model with two approaches: pure pursuit and model predictive control. Their model is as follows:

$$\begin{aligned}
&\ddot{x} = \dot{\psi}\dot{y} + a_x,\\
&\ddot{y} = -\dot{\psi}\dot{x} + \frac{2}{m}\left(F_{c_f}\cos\left(\delta_f\right) + F_{c_r}\right),\\
&\ddot{\psi} = \frac{2}{I_z}\left(l_f F_{c_f} - l_r F_{c_r}\right),\\
&\dot{X} = \dot{x}\cos\left(\psi\right) - \dot{y}\sin\left(\psi\right),\\
&\dot{Y} = \dot{x}\sin\left(\psi\right) + \dot{y}\cos\left(\psi\right),
\end{aligned} \tag{55}$$

where, the longitudinal and lateral speed is represented by x and y, respectively, with respect to the body frame. The lateral forces on the front and back wheel are denoted by F_{c_r} and F_{c_f}, respectively. The yaw rate, vehicle's mass, and yaw inertia are denoted by $\dot{\psi}, m$, and I_z, respectively. For the linear tire model, the F_{c_i} is defined by the equation

$$F_{c_i} = -C_{\alpha_i}\alpha_i, \tag{56}$$

where, $i \in f, r$ and α_i is the slip angle given by equation (12)-(13) and C_{α_i} is the tire cornering stiffness.

$$\alpha_f = \arctan\left(\frac{v_y + l_f\dot{\psi}}{v_x}\right) - \delta \tag{57}$$

$$\alpha_r = \arctan\left(\frac{v_y - l_r\dot{\psi}}{v_x}\right), \tag{58}$$

In this model the speed of the differential module is synthesized by the speeds of left and right driving wheels, and the speeds of the two differential modules can be written as [19]:

$$\begin{cases} v_f = \left(v_{fr} + v_{fl}\right)/2 \\ v_r = \left(v_{rr} + v_{rl}\right)/2 \end{cases} \tag{59}$$

The prerequisite for the steering of the differential module is that it has a certain angular velocity, which is realized by the speed difference between the two driving wheels of the differential module. Set the speed difference between the two driving wheels of the front differential module to be Δv_f, and the rear differential module to be Δv_r; then the speed of the four driving wheels can be written as:

$$\begin{cases} v_{fr} = vf + \Delta v_f/2 \\ v_{fl} = v_f - \Delta v_f/2 \\ v_{rr} = v_r + \Delta v_r/2 \\ v_{rl} = v_r - \Delta v_r/2 \end{cases} \tag{70}$$

The angular velocity of the two differential modules ω_f, ω_r, can be written as:

$$\begin{cases} \omega_f = \frac{|v_{fr} - v_{fl}|}{D} = \frac{|\Delta v_f|}{D} \\ \omega_r = \frac{|v_{rr} - v_{rl}|}{D} = \frac{|\Delta v_r|}{D} \end{cases} \tag{71}$$

The velocity components $\mathcal{V}_{fx}, \mathcal{V}_{fy}$ of $\mathcal{V}_f$ on the x and y axes are:

$$\begin{cases} v_{fx} = v_f \cdot \sin\left|\theta_f\right| \\ v_{fy} = v_f \cdot \cos\left|\theta_f\right| \end{cases} \tag{72}$$

The velocity components v_{rx}, v_{ry} of v_r on the x and y axes are:

$$\begin{cases} v_{rx} = v_r \cdot \sin\left|\theta_r\right| \\ v_{ry} = v_r \cdot \cos\left|\theta_r\right| \end{cases} \tag{73}$$

The speeds of AGV centre on the x and y axes are:

$$\begin{cases} v_y = v_{fy} = v_{ry} \\ v_x = v_{fx} - v_{rx} \end{cases} \tag{74}$$

The steering of the AGV is caused by the sub-speed of v_f and v_r on the x-axis (two sub-speeds are reversed), and the angular velocity of AGV center can be written as :

$$\omega_c = \frac{|v_{rx}| + |v_{fx}|}{L} = \frac{|v_r \cdot \sin|\theta_r|| + |v_f \cdot \sin|\theta_f||}{L} \tag{75}$$

Another mathematical model [20] developed for the wheeled robot by Lagrange or Newton Euler equation. In the dynamics model, F and M are the fore and torque generated by wheel system, the output variable is body coordinates $(x_1, x_2) \in R^2$ and azimuth angle α , the input variables are longitudinal force acted on wheels and control signal u_θ^i of wheels. For simplicity, it was assumed that: the body of the robot is rigid body; the contact type between wheel system and land is point contact. The development of the wheeled mobile robot: the wheel system is installed on the body of robot. The position of the robot in Cartesian coordinate system $X \in R^2$ is represented by vector $x = (x_1, x_2)$. The point C is the centric of the robot, angle α is azimuth angle. In the Y axis, the movement of the wheeled mobile robot can be described as

$$\dot{\mathrm{x}} = V, m\dot{V} = F, \dot{\alpha} = \omega, J\dot{\omega} = M \tag{76}$$

Where $V \in R^2$-absolute linear velocity, $F = (F_V, F_T)$: external force, ω : angular velocity, M : torque, m : mass, J : moment of inertia. In order to analysis the velocity and

force in relative coordinate system, the following matrix was introduced:

$$T(\alpha) = \begin{vmatrix} \cos\alpha & \sin\alpha \\ -\sin\alpha & \cos\alpha \end{vmatrix} \quad (77)$$

The linear velocity of C_i can be calculated by

$$V^i = \begin{vmatrix} V_V^i \\ V_T^i \end{vmatrix} = T(\theta^i)\left(V_p + \omega E^T z^i\right) \quad (78)$$

Where V_p-velocity of robot body, V_V^i-vertical velocity of wheel i, V_T^i-tangential velocity of wheel i.
So the kinematics model of the mobile robot is

$$\begin{vmatrix} \dot{x} \\ \dot{\alpha} \end{vmatrix} = \begin{vmatrix} V \\ \omega \end{vmatrix}, J\begin{vmatrix} \dot{V} \\ \dot{\omega} \end{vmatrix} = R^T(\alpha)\begin{vmatrix} F_p \\ M \end{vmatrix}, u = \begin{vmatrix} V_V^T \\ d_j^T \end{vmatrix}\begin{vmatrix} -1 \\ V_p^T F_p + \omega M \\ 0 \end{vmatrix}, \begin{vmatrix} F_p \\ M \end{vmatrix} = T_1(\theta)u + T_2(\theta)f$$
$$f = -k_f V_T = -k_f T_2(\theta)\begin{vmatrix} V_p \\ \omega \end{vmatrix}, \dot{\theta} = K_\theta u_\theta \quad (79)$$

Where, $R(\alpha) = \begin{vmatrix} T(\alpha) & 0 \\ 0 & 1 \end{vmatrix}, J = \begin{vmatrix} m & 0 \\ 0 & J \end{vmatrix}$; u_θ-control signal, $u_\theta = (u_\theta^1, u_\theta^1, \cdots u_\theta^n)$; K_θ - matrix of transmission coefficient, $K_\theta = \text{diag}\,(k_\theta^1, k_\theta^2, \cdots, k_\theta^n)$; u-vertical force of drive wheel, $u = (u^1, \cdots, u^n)$; f-tangential friction, $f = (f^1, \cdots, f^n)$; k_f-tangential friction coefficient. Control model of wheeled mobile robot. Path Following of wheel mobile robot requires the robot to follow a predefined path with an expected velocity. The force acted on the body to follow a path can be calculated by

$$F_p = mT(\Delta\alpha)\begin{vmatrix} u_s \\ u_d \end{vmatrix}, M = J\left(\eta u_s + u_\gamma\right) \quad (80)$$

Where $u_s = \alpha^* + k_{s1}\Delta\dot{s} + k_{s2}\Delta s$-vertical control, $u_d = \eta\dot{s}^2 - k_{d1}\dot{d} - k_{d2}d -$ tangential control,
$u_\gamma = \dot{\eta}\dot{s} - k_{\gamma 1}\dot{\delta} - k_{\gamma 2}\delta, -$ angle control,

$k_{s1}, k_{s2}, k_{d1}, k_{d2}, k_{\gamma 1}, k_{\gamma 2}$ - coefficients, s - displacement, d-path error, γ-azimuth error. s, d, γ can be got by sensor or calculation. The vertical force u acted on wheel system and control angle u_θ to turn the wheel's direction can be calculated by,

$$u_\theta = \text{diag}\left\{\frac{1}{V_V^i}\right\}\left(T_2^T J^{-1}\begin{vmatrix} F_p \\ M \end{vmatrix} - \omega T_1^T\begin{vmatrix} V_p \\ 0 \end{vmatrix}\right) \quad (81)$$

$$u = \begin{vmatrix} V_V^T \\ d_i^T \end{vmatrix}^{-1}\begin{vmatrix} V_p^T F_p + \omega M \\ 0 \end{vmatrix} \quad (82)$$

2.4 Four Wheel Skid Steering AGVs

The Skid Steering is a movement mechanism widely used in mobile robots. For the skid steered robot, as shown in figure 5, there is no steering mechanism, and the direction of Movement is changed by turning the wheels left and right at different speeds. The design of the mechanism makes the robot mechanically robust and easy to navigate outdoors. Due to the complex wheel/ground interaction and kinematic constraints, it remains difficult to obtain precise kinematic and dynamic models for sliding guided mobile robots [21].

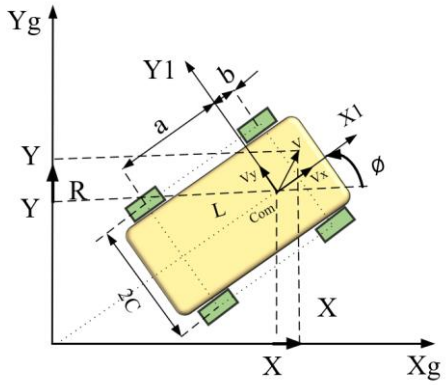

Figure 5. 4-wheel Skid Steering Robot Schematics.

The mathematical model of 4-wheel skid-steering mobile robot in a systematic way [22].in the proposed model, the active force Fi and reactive force Ni are related that F_i is dependent linearly on the wheel control input $\bar{\tau}_i$, namely,

$$F_i = \frac{\tau_i}{r} \quad (83)$$

Assuming that the vertical force N_i acts from the surface to the wheel. Considering the four wheels of the vehicle and neglecting additional dynamic properties, obtained are the following equations of equilibrium:

$$\begin{aligned} N_1 a &= N_2 b, \\ N_4 a &= N_3 b, \\ \textstyle\sum_{i=1}^{4} N_i &= mg, \end{aligned} \quad (84)$$

where m denotes the vehicle mass, and g is the gravity acceleration. Since there is symmetry along the longitudinal midline,

$$\begin{aligned} N_1 = N_4 &= \frac{b}{2(a+b)}mg \\ N_2 = N_3 &= \frac{a}{2(a+b)}mg \end{aligned} \quad (85)$$

Assume that the vector F_{si} results from the rolling resistant moment τ_{ri} and the vector F_{li} denotes the lateral reactive force. These reactive forces can be regarded as friction ones. However, it is important to note that friction modeling is quite complicated since it is highly nonlinear

and depends on many variables. Therefore, in most cases, only a simplified approximation describing the friction F_f as a superposition of Coulumb and viscous friction is considered. It can be written as

$$F_f(\sigma) = \mu_c N \text{sgn}\,(\sigma) + \mu_v \sigma, \tag{86}$$

where σ denotes the linear velocity, N is the force perpendicular to the surface, while μ_c and μ_v denote the coefficients of Coulumb and viscous friction, respectively. Since for the SSMR the velocity σ is relatively low, especially during lateral slippage, the relation $\mu_c N"|\mu_v \sigma|$ is valid, which allows to neglect the term $\mu_v \sigma$ to simplify the model. It is critical to emphasize that the function (xx) is not smooth when the velocity σ equals zero because of the sign function sgn (σ). It is obvious that this function is not differentiable at $\sigma = 0$. Since a continuous and time differentiable model of the SSMR should be obtained, the following approximation of this function is proposed:

$$\widehat{\text{sgn}}(\sigma) = \frac{2}{\pi}\arctan\,(k_s \sigma) \tag{87}$$

where $k_s"1$ is a constant which determines the approximation accuracy according to the relation

$$\lim_{k_s \to \infty} \frac{2}{\pi}\arctan\,(k_s \sigma) = \text{sgn}\,(x). \tag{88}$$

Based on the previous deliberations, the friction forces for one wheel can be written as

$$\begin{aligned} F_{li} &= \mu_{lci} m g \widehat{\text{sgn}}(v_{yi}) \\ F_{si} &= \mu_{sci} m g \widehat{\text{sgn}}(v_{xi}) \end{aligned} \tag{89}$$

where μ_{lci} and μ_{sci} denote the coefficients of the lateral and longitudinal forces, respectively.

Using the Lagrange-Euler formula with Lagrange multipliers to include the nonholonomic constraint, the dynamic equation of the robot can be obtained. Next, it is assumed that the potential energy of the robot $PE(q) = 0$ because of the planar motion. Therefore, the Lagrangian L of the system equals the kinetic energy:

$$L(\boldsymbol{q}, \dot{\boldsymbol{q}}) = T(\boldsymbol{q}, \dot{q}). \tag{90}$$

Considering the kinetic energy of the vehicle and neglecting the energy of rotating wheels, the following equation can be developed:

$$T = \frac{1}{2} m v^T v + \frac{1}{2} I \omega^2 \tag{91}$$

where m denotes the mass of the robot and I is the moment of inertia of the robot about the COM. For simplicity, it is assumed that the mass distribution is homogeneous. Since $v^T v = v_x^2 + v_y^2 = \dot{X}^2 + \dot{Y}^2$, Equation (90) can be rewritten as follows:

$$T = \frac{1}{2} m (\dot{X}^2 + \dot{Y}^2) + \frac{1}{2} I \dot{\theta}^2 \tag{92}$$

After calculating the partial derivative of kinetic energy and its time-derivative, the inertial forces can be obtained as

$$\frac{\mathrm{d}}{\mathrm{d}t}\left(\frac{\partial E_k}{\partial \dot{q}}\right) = \begin{bmatrix} m\ddot{X} \\ m\ddot{Y} \\ I\ddot{\theta} \end{bmatrix} = M\ddot{q} \tag{93}$$

where

$$M = \begin{bmatrix} m & 0 & 0 \\ 0 & m & 0 \\ 0 & 0 & I \end{bmatrix}$$

Consequently, the forces which cause the dissipation of energy are considered. The following resultant forces expressed in the inertial frame can be calculated:

$$\begin{aligned} F_{rx}(\dot{q}) &= \cos\,\theta \sum_{i=1}^{4} F_{si}(v_{xi}) - \sin\,\theta \sum_{i=1}^{4} F_{li}(v_{yi}) \\ F_{ry}(\dot{q}) &= \sin\,\theta \sum_{i=1}^{4} F_{si}(v_{xi}) + \cos\,\theta \sum_{i=1}^{4} F_{li}(v_{yi}) \end{aligned} \tag{94}$$

The resistive moment around the mass centre M_r can be calculated as

$$\begin{aligned} M_r(\dot{q}) = \; & -a \sum_{i=1,4} F_{li}(v_{yi}) + b \sum_{i=2,3} F_{li}(v_{yi}) \\ & + c\left[-\sum_{i=1,2} F_{si}(v_{xi}) + \sum_{i=3,4} F_{si}(v_{xi})\right]. \end{aligned} \tag{94}$$

To define generalized resistive forces, the vector

$$R(\dot{q}) = [F_{rx}(\dot{q}) \quad F_{ry}(\dot{q}) \quad M_r(\dot{q})]^T \tag{95}$$

is introduced. The active forces generated by the actuators that make the robot move can be presented in the inertial frame as follows:

$$\begin{aligned} F_x &= \cos\,\theta \sum_{i=1}^{4} F_i, \\ F_y &= \sin\,\theta \sum_{i=1}^{4} F_i. \end{aligned} \tag{96}$$

The active torque around the COM is calculated as

$$M = c(-F_1 - F_2 + F_3 + F_4). \tag{97}$$

In consequence, the vector F of active forces has the following form:

$$\boldsymbol{F} = [F_x \quad F_y \quad M]^T \tag{98}$$

Assume that each wheel's radius is the same then,

$$\boldsymbol{F} = \frac{1}{r}\begin{bmatrix} \cos\,\theta \sum_{i=1}^{4} \tau_i \\ \sin\,\theta \sum_{i=1}^{4} \tau_i \\ c(-\tau_1 - \tau_2 + \tau_3 + \tau_4) \end{bmatrix} \tag{99}$$

To simplify the notation, a new torque control input τ is defined as

$$\tau = \begin{bmatrix}\tau_L \\ \tau_R\end{bmatrix} = \begin{bmatrix}\tau_1 + \tau_2 \\ \tau_3 + \tau_4\end{bmatrix} \quad (100)$$

where τ_L and τ_R signify the torques generated by the wheels on the vehicle's left and right sides, respectively. Combining (99) and (100), we get

$$F = B(q)\tau, \quad (101)$$

where B is the input transformation matrix defined as

$$B(q) = \frac{1}{r}\begin{bmatrix}\cos\theta & \cos\theta \\ \sin\theta & \sin\theta \\ -c & c\end{bmatrix} \quad (102)$$

Next, using (92), (95) and (101), the following dynamic model is obtained:

$$M(q)\ddot{q} + R(\dot{q}) = B(q)\tau. \quad (103)$$

It should be noted that (103) describes the dynamics of a free body only and does not include the nonholonomic constraint. Therefore, a constraint has to be imposed on (103). To this end, a vector of Lagrange multipliers, λ, is introduced as follows:

$$M(q)\ddot{q} + R(\dot{q}) = B(q)\tau + A^T(q)\lambda. \quad (104)$$

For control purposes, it would be more suitable to express (104) in terms of the internal velocity vector $\boldsymbol{\eta}$. Therefore, (104) is multiplied from the left by $S^T(q)$, which results in

$$\begin{aligned} S^T(q) \quad & M(q)\ddot{q} + S^T(q)\mathbf{R}(\dot{q}) \\ & = S(q)^T B(q)\tau + S^T(q)A^T(q)\lambda. \end{aligned} \quad (105)$$

After taking the time derivative,

$$\ddot{q} = \dot{S}(q)\eta + S(q)\dot{\eta}. \quad (106)$$

Hence, combining (106) and (104), the dynamic equations become

$$\bar{M}\dot{\eta} + \bar{C}\eta + \bar{R} = \bar{B}\tau \quad (107)$$

Where,

$$\bar{C} = S^T M\dot{S} = mx_{\text{ICR}}\begin{bmatrix}0 & \dot{\theta} \\ -\dot{\theta} & \dot{x}_{\text{ICR}}\end{bmatrix} \quad (108)$$

$$\bar{M} = S^T MS = \begin{bmatrix}m & 0 \\ 0 & mx_{\text{ICR}}^2 + I\end{bmatrix} \quad (109)$$

$$\bar{R} = S^T R = \begin{bmatrix}F_{rx}(\dot{q}) \\ x_{\text{ICR}}F_{ry}(\dot{q}) + M_r\end{bmatrix} \quad (110)$$

$$\bar{B} = S^T B = \frac{1}{r}\begin{bmatrix}1 & 1 \\ -c & c\end{bmatrix} \quad (111)$$

To have a better model [23] propose a kinematic approach for tracked mobile robots in order to improve motion control and pose estimation. (V_l, V_r) is the linear velocity of the robot's left and right tracks in relation to the robot frame. Then, on the plane, direct kinematics can be described as follows:

$$(v_x, v_y, \omega_z) = f_d(V_l, V_r) \quad (112)$$

where $\mathbf{v} = (v_x, v_y)$ is the translational velocity of the vehicle in relation to its local frame, and ω_z is its angular velocity. Conversely, finding control actions that result in the desired motion can be expressed as the inverse kinematics problem:

$$(V_l, V_r) = f_i(v_x, v_y, \omega_z). \quad (113)$$

Local coordinates for the vehicle and track ICRs can be obtained geometrically as a function of the vehicle's angular and translational velocities as

$$x_{ICR_v} = \frac{-v_y}{\omega_z} \quad (114)$$

$$x_{ICRl} = \frac{V_l - v_y}{\omega_z} \quad (115)$$

$$y_{ICR_v} = y_{ICRI} = y_{ICRr} = \frac{v_x}{\omega_z}. \quad (116)$$

Instantaneous translational and rotational speeds with respect to the local frame can be obtained as

$$\begin{aligned} v_x &= \frac{V_r - V_l}{x_{ICRr} - x_{ICRI}} y_{ICRv} \\ v_y &= \frac{V_r + V_l}{2} - \frac{V_r - V_l}{x_{ICRr} - x_{ICRl}}\left(\frac{x_{ICRr} + x_{ICRl}}{2}\right) \\ \omega_z &= \frac{V_r - V_l}{x_{ICRr} - x_{ICRl}} \end{aligned} \quad (117)$$

These equations represent the vehicle's direct kinematics assuming that the ICRs of the left and right treads could be properly estimated. If the ICRs lie precisely on the local X-axis (i.e., $y_{ICRv} = 0$), then the vehicle's velocity $\mathbf{v}$ has no transversal component (i.e., $v_x = 0$).On the other hand, inverse kinematic relations can be expressed by

$$\begin{aligned} V_l &= v_y + x_{ICRl}\omega_z \\ V_r &= v_y + x_{ICRr}\omega_z, \end{aligned} \quad (118)$$

which includes a non-holonomic restriction, since v_x references cannot be directly imposed. Besides, according to these equations, the same control input values are computed regardless of y_{ICRv} in the model. The inverse of the normalized distance between the wheels can be used to calculate the vehicle's steering efficiency index χ. track ICRs

$$\chi = \frac{L}{x_{ICRr} - x_{ICRl}}; (0 < \chi \leqslant 1), \quad (119)$$

L is the distance between the centrelines of the two tracks. When there is no slippage, the index equals 1 (i.e., ideal differential drive). Similarly, a normalized eccentricity index can be defined as follows:

$$e = \frac{x_{ICRr} + x_{ICRl}}{x_{ICRr} - x_{ICRl}} \quad (120)$$

Index e is zero when track ICRs are symmetrical with respect to the local Y-axis. For friction, in the case of hard-surface soils, the resulting force for a point in the track is a function of its slip velocity $\mathbf{v}_s$ as expressed by Coulomb's law

$$\tau = -[\mu] p \frac{v_s}{|v_s|} \quad (121)$$

where p is the pressure under the track, and $[\mu]$ is a coefficient matrix, which, in the general case of anisotropic friction on the XY plane, has the following form:

$$[\mu] = \begin{bmatrix} \mu_x & 0 & 0 \\ 0 & \mu_y & 0 \\ 0 & 0 & 0 \end{bmatrix}. \quad (122)$$

Moreover, if the inertia frame coincides with the vehicle frame, [**I**] is a diagonal matrix expressed as

$$[\mathbf{I}] = \begin{bmatrix} I_x & 0 & 0 \\ 0 & I_y & 0 \\ 0 & 0 & I_z \end{bmatrix}. \quad (123)$$

2.5 Six Wheel AGVs

Six-wheel AGVs have three wheels on each side, totalling six wheels to guide it on its path automatically. All the wheels run at different speeds and power to control the vehicle's steering. [24]

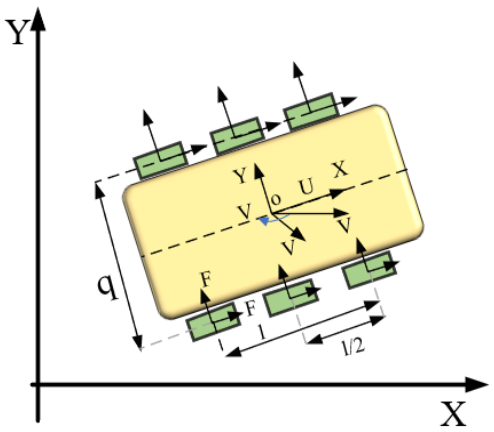

Figure 6. Six-wheel AGV schematic

The above figure 6 shows the schematics of an example six-wheel AGV. This model is represented by [25] as shown in equation (124)

$$\begin{aligned} \dot{\xi}_r &= R(\theta) \cdot \dot{\xi} \\ \dot{\xi} &= \{\dot{x} \quad \dot{y} \quad \dot{\theta}\}^T \\ \dot{\xi}_r &= \{\dot{x}_r \quad \dot{y}_r \quad \dot{\theta}_r\}^T \\ R(\theta) &= \begin{bmatrix} c\theta & s\theta & 0 \\ -s\theta & c\theta & 0 \\ 0 & 0 & 1 \end{bmatrix} \end{aligned} \quad (125)$$

The wheel variables model (125) shows the orientation to the robot's coordinate system xr, yr as observed by the inertial coordinate system x,y, Ĥ is the robot's linear velocity, and r is the location relative to the inertial coordinate system. The angular velocity of the wheel is φ_1, φ_2.

$$\begin{aligned} \dot{\xi} &= R(\theta)^{-1} \cdot \dot{\xi}_r \\ \dot{\xi} &= \{\dot{x}\dot{y}\dot{\theta}\}^T = f(l, r, \theta, \varphi_1, \varphi_2) \\ \dot{\xi}_r &= \{\dot{x}_r \dot{y}_r \dot{\theta}_r\}^T \end{aligned} \quad (126)$$

$$\xi = \begin{bmatrix} c\theta & -s\theta & 0 \\ s\theta & c\theta & 0 \\ 0 & 0 & 1 \end{bmatrix} \begin{Bmatrix} \dot{x}_r \\ \dot{y}_r \\ \dot{\theta}_r \end{Bmatrix} = \begin{bmatrix} c\theta & -s\theta & 0 \\ s\theta & c\theta & 0 \\ 0 & 0 & 1 \end{bmatrix} \begin{Bmatrix} \frac{r\dot{\varphi}_1}{2} + \frac{r\dot{\varphi}_2}{2} \\ \frac{\dot{\varphi}_1}{2.l} \quad -\frac{r\dot{\varphi}_2}{2.l_r} \end{Bmatrix} \quad (127)$$

The dynamic model concerning robot coordinate system:

$$\begin{aligned} \frac{d}{dt}(m\vec{v}) &= \sum F_{Ext} \\ \frac{d}{dt}(m\vec{v}) + \vec{w} \times (m\vec{v}) &= \sum F_{Ext} \\ m\begin{Bmatrix} a_x \\ a_y \\ a_z \end{Bmatrix} + \begin{Bmatrix} w_x \\ w_y \\ w_z \end{Bmatrix} \times m\begin{Bmatrix} v_x \\ v_y \\ v_z \end{Bmatrix} &= \begin{Bmatrix} \sum F_x \\ \sum F_y \\ \sum F_z \end{Bmatrix} \\ m\begin{Bmatrix} a_x + v_z w_y - v_y w_z \\ a_y + v_x w_z - v_z w_y \\ a_z + v_y w_x - v_x w_y \end{Bmatrix} &= \begin{Bmatrix} \sum F_x \\ \sum F_y \\ \sum F_z \end{Bmatrix} \end{aligned} \quad (128)$$

In this case, considering non-slip condition and movement at the plane (x, y) the equation system is:

$$m\begin{Bmatrix} \ddot{x}_r \\ \dot{x}_r \dot{\theta}_r \\ 0 \end{Bmatrix} = \begin{Bmatrix} F_{fx} \\ F_{fy} \\ N - mg \end{Bmatrix} \quad (129)$$

.In function of wheel variables, is presented the equation system :

$$m\begin{Bmatrix} \frac{r\dot{\varphi}_1}{2} + \frac{r\dot{\varphi}_1}{2} \\ \frac{r^2\dot{\varphi}_1^2}{4l} + \frac{r^2\dot{\varphi}_2^2}{4l} \\ 0 \end{Bmatrix} = \begin{Bmatrix} F_{fx} \\ F_{fy} \\ N - mg \end{Bmatrix} \quad (130)$$

The moment equations to the robot, are described at equations where I is the inertia tensor of robot:

$$\frac{d}{dt}(I\vec{w}) = \Sigma M_{Ext}$$
$$\frac{d}{dt}(Y\vec{w}) + \vec{w} \times (I\vec{w}) = \Sigma M_{Ext}$$
$$I\begin{Bmatrix}\alpha_x\\ \alpha_y\\ \alpha_z\end{Bmatrix} + \begin{Bmatrix}w_x\\ w_y\\ w_z\end{Bmatrix} \times \left(\begin{Bmatrix}v_x\\ v_y\\ v_z\end{Bmatrix} = \begin{matrix}\sum M_x\\ \sum M_y\\ \left(\sum M_z\right)\end{matrix} \right. \quad (131)$$
$$\begin{bmatrix} I_{xx} & -I_{xy} & -I_{xz} \\ -I_{xy} & I_{yy} & -I_{yz} \\ -I_{xz} & -I_{yz} & I_{zz} \end{bmatrix} \begin{Bmatrix}\alpha_x\\ \alpha_y\\ \alpha_z\end{Bmatrix} + \begin{Bmatrix}w_x\\ w_y\\ w_z\end{Bmatrix} \times$$
$$\begin{bmatrix} I_{xx} & -I_{xy} & -I_{xz} \\ -I_{xy} & I_{yy} & -I_{yz} \\ -I_{xz} & -I_{yz} & I_{zz} \end{bmatrix} \begin{Bmatrix}v_x\\ v_y\\ v_z\end{Bmatrix} = \begin{matrix}\sum M_x\\ \sum M_y\\ \left(\sum M_z\right)\end{matrix}$$

The robot will be symmetric at plane (zr, xr) and (zr, yr) thus the inertia tensor is a diagonal matrix I_{xx}.

$$\begin{bmatrix} I_{xx} & 0 & 0 \\ 0 & I_{yy} & 0 \\ 0 & 0 & I_{zz} \end{bmatrix} \begin{Bmatrix}\alpha_x\\ \alpha_y\\ \alpha_z\end{Bmatrix} + \begin{Bmatrix}w_x\\ w_y\\ w_z\end{Bmatrix} \times \begin{bmatrix} I_{xx} & 0 & 0 \\ 0 & I_{yy} & 0 \\ 0 & 0 & I_{zz} \end{bmatrix} \begin{Bmatrix}v_x\\ v_y\\ v_z\end{Bmatrix} = \begin{matrix}\sum M_x\\ \sum M_y\\ \left(\sum M_z\right)\end{matrix}$$
$$\begin{Bmatrix} I_{xx} & \alpha_x \\ I_{yy} & \alpha_y \\ I_{zz} & \propto_z \end{Bmatrix} + \begin{Bmatrix} w_y I_{zz} v_z - w_z I_{yy} v_y \\ w_z I_{xx} v_x - w_x I_{zz} \\ w_x I_{yy} v_x - w_y I_{xx} v_x \end{Bmatrix} = \begin{matrix}\sum M_x\\ \sum M_y\\ \left(\sum M_z\right)\end{matrix} \quad (132)$$

With non-slip conditions and movement only at the plane (x, y) the equations system is:

$$\begin{Bmatrix} 0 \\ 0 \\ I_{zz} \propto_z \end{Bmatrix} + \begin{Bmatrix} 0 \\ w_z I_{xx} v_x \\ 0 \end{Bmatrix} = \begin{Bmatrix} N_{\text{left}}\, l - N_{\text{rigth}}\, l \\ N_{\text{back}}\, d - N_{\text{front}}\, d + T_{\text{motor}} \\ F_{fxrigth} l - F_{fxleft} l - F_{fy\ \text{front}}\, d - F_{fyleft} d \end{Bmatrix} \quad (133)$$

In function of wheel variables and dimensions of robot, is presented the equations:

$$\begin{Bmatrix} 0 \\ 0 \\ I_{zz}\ddot{\theta}_r \end{Bmatrix} + \left\{ I_{xx} \begin{bmatrix} \frac{r^2\dot{\varphi}_1^2}{4l} + \frac{r^2\dot{\varphi}_2^2}{4l} \\ 0 \end{bmatrix} \right\} = \begin{Bmatrix} (N_{left} - N_{\text{rigth}})l \\ (N_{\text{back}} - N_{front})d + T_{\text{motori}} \\ (F_{fxrigth} - F_{fxleft})l - (F_{fyfront} + F_{fy\ \text{back}})d \end{Bmatrix} \quad (134)$$

For this robot type (six-wheel mobile robot), the dynamic equation of the high-speed motion [14] is shown in equation (134).

$$mV_x(\dot{\beta} + \gamma) = \Sigma_{i=1}^{6} F_{yi} \quad (135)$$
$$I_z\dot{\gamma} = \left[\frac{b}{2}(F_{x2} + F_{x4} + F_{x6} - F_{x1} - F_{x3} - F_{x5})\right] + \left[\frac{l}{2}(F_{y1} + F_{y2}) - \frac{l}{2}(F_{y5} + F_{y6})\right] \quad (136)$$
$$M_z = \frac{d}{2}(F_{x2} + F_{x4} + F_{x6} - F_{x1} - F_{x3} - F_{x5})$$
$$M_d = \frac{l}{2}(F_{y1} + F_{y2}) - \frac{l}{2}(F_{y5} + F_{y6})$$

Where m is the mass of the mobile robot V_x is the longitudinal speed of the mobile robot β is the sliding angle, and the moment of inertia γ is the yaw rate d is the distance between the left and right wheels, and F_{xi} is the longitudinal force of the tire. The direct yaw moment M_z produced by the longitudinal driving force difference between the tires the steering moment M_d produced as the resistance component of the tires during turning, together form the yaw moment [26].The steady-state steering angle when driving on the road with a turning radius of R is:

$$\delta = \frac{l}{R} + K_v a_y \quad (137)$$

Where K_V is the under-steer gradient, and the formula is as follows:

$$K_v = \frac{m}{4C_{\alpha f}} - \frac{m}{4C_{\alpha r}}$$
$$\frac{1}{R} = \frac{\delta}{l + \frac{mV_x^2(lC_{\alpha r} - lC_{\alpha f})}{4lC_{\alpha r}C_{\alpha f}}} \quad (138)$$

The vertical force of the tire changes with the longitudinal acceleration a_y and the lateral acceleration a_x,

$$F_{z1} = \frac{mg}{6} - \frac{m_s a_x h_s}{2l} - k_f \frac{m_s a_y h_s}{d}$$
$$F_{z2} = \frac{mg}{6} - \frac{m_s a_x h_s}{2l} + k_f \frac{m_s a_y h_s}{d}$$
$$F_{z3} = \frac{mg}{6} - k_m \frac{m_s a_y h_s}{d}$$
$$F_{z4} = \frac{mg}{6} + k_m \frac{m_s a_y h_s}{d} \quad (139)$$
$$F_{z5} = \frac{mg}{6} + \frac{m_s a_x h_s}{2l} - k_r \frac{m_s a_y h_s}{d}$$
$$F_{z6} = \frac{mg}{6} + \frac{m_s a_x h_s}{2l} + k_r \frac{m_s a_y h_s}{d}$$

Where m is the sprung mass, h_s is the sprung mass height. g is the gravitational constant k_f and k_r are the lateral weight offset distributions of the front and rear wheels, respectively.

The absolute speed of mobile robots $[\dot{x} \quad \dot{y} \quad \dot{\theta}]^T$ converted in the local coordinate system to $[\dot{u} \quad \dot{v} \quad \dot{r}]^T$:

$$\begin{bmatrix}\dot{x}\\ \dot{y}\\ \dot{\theta}\end{bmatrix} = \begin{bmatrix}\cos\theta & -\sin\theta & 0\\ \sin\theta & \cos\theta & 0\\ 0 & 0 & 1\end{bmatrix}\begin{bmatrix}u\\ v\\ r\end{bmatrix} \quad (140)$$

Among them, u represents the x-axis velocity component of the unmanned platform in the local coordinate system, v represents the y-axis velocity component, and r represents the angular velocity. Analyse and calculate the rotational movement of the six wheels of the mobile robot, and obtain the equation of motion as:

$$\begin{cases} J_i\dot{\omega}_i = T_{ei} - F_{xi}R - T_{fi} \\ T_{fi} = F_{fi}R \end{cases} \quad (141)$$

2.6 Ackermann AGV

Rudolph Ackermann invented the Ackermann in 1816. The steering is based on different steering angles for the left and right wheels of a steering axis. In automotive implementations, this is realized by dedicated mechanics shown on the right side of the picture. Each wheel's steering angle (also called Ackermann Angle) depends on the vehicle's dimensions [27]. Land vehicles generally have two types of steering mechanisms. Differential (or non-slip) steering and Ackerman steering. Either way, one of the biggest problems with differential steering is that it wastes energy dragging the wheels across the ground. Ackermann steering is often present in the car, which allows the wheels to turn around at similar turning points. The wheels do not slip sideways when turning; Therefore, energy is not wasted while spinning [28] .

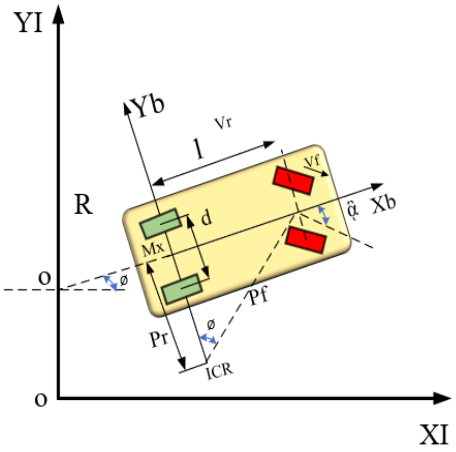

Figure 7. Ackermann AGV Schematics

Figure 7 shows the Ackermann AGV and variables for the upcoming below models. Based on the model [29] Ackermann described, AGV has the kinematic structure of an automobile, two front wheels with the same turning angle φ and two parallel non-steered back wheels. However, this kinematics model is not as the same as the practical vehicles. Practical vehicles have Ackerman steering linkage between the two front wheels, and this principle approximately ensures the actuator coupling criterion by providing the correct wheel angles to avoid wheel side slip. Define φ_2 as the turning angle of the inner tire and φ_1 as outer tire. In order to ensure that the vehicle turning without transverse slip, four wheels should rotate at ICR, besides, φ_1 and φ_2 need to satisfy equation (142).

$$\begin{cases} \cot\ \varphi_1 = \cot\ \varphi + d/2l \\ \cot\ \varphi_2 = \cot\ \varphi - d/2l \end{cases} \quad (142)$$

Then we can get equation (142):

$$\cot\ \varphi_1 - \cot\ \varphi_2 = \frac{\rho_r + d/2}{l} - \frac{\rho_r - d/2}{l} = \frac{d}{l} \quad (143)$$

Define ρ_f^l is ICR radius of the left front wheel, ρ_f^r is ICR radius of the right front wheel, ρ_r^l is ICR radius of the left rear wheel and ρ_r^r is ICR radius of the right rear wheel, then we testify $\rho_f^l = l/\sin\ \varphi_1, \rho_f^r = l/\sin\ \varphi_2, \rho_r^l = l/\tan\ \varphi + d/2$, and $\rho_r^r = l/\tan\ \varphi - d/2$. Define inner minus $\Delta\rho$ as $\rho_f^l - \rho_r^l$ when turning right (when the vehicle turns left $\Delta\rho$ equals $\rho_f^r - \rho_r^r$). Different influences on vehicles, such as side slip, brake, and slide, are neglected in the assumptions. But practically, these instances always happen to vehicles, which declare the nonholonomic restriction is destroyed and do not satisfy.

$$\dot{x}\sin\ \theta - \dot{y}\cos\ \theta = 0 \quad (144)$$

Assuming e_r^R as error vector of the rear wheel, it can be defined by $\sigma \cdot [x_e \quad y_e \quad \varphi_e]^T \cdot x_e(t), y_e(t)$ and $\varphi_e(t)$ change by time $t. \sigma$ is error plus, commonly, $\sigma = 1. c$ is error of turning angle φ.

$$\dot{\zeta}_r^R = \left[v_r + \dot{x}_e \quad \dot{y}_e \quad \frac{\tan(\varphi+\varphi_e)}{l} v_r\right]^T \quad (145)$$

$$\dot{\zeta}_r^I = \left[v_r\cos\ \theta \quad v_r\sin\ \theta \quad \frac{v_r}{l}\tan\ \varphi\right]^T + [\dot{x}_e\cos\ \theta - y_e\sin\ \theta \quad \dot{x}_e\sin\ \theta + \dot{y}_e\cos\ \theta \quad \phi_e]^T \quad (146)$$

In equation ϕ_e is defined:

$$\phi_e = \frac{v_r}{l} \cdot \frac{\tan\ \varphi_e(1+\tan^2\ \varphi)}{1-\tan\ \varphi \cdot \tan\ \varphi_e} \quad (146)$$

When errors and other factors destroy nonholonomic restriction of vehicle, the range can be declared by κ_x and κ_y. $K_x = x_e\cos\ \theta - y_e\sin\ \theta, \kappa_y = x_e\sin\ \theta + y_e\cos\ \theta$, which map position error from local coordinate frame to global coordinate frame. Let $e_r^I = [\kappa_x \quad \kappa_y]^T$, and e_r^I has no relation to the vehicle status but is influenced by different kinds of errors. If not take proper measures to control the accumulation of error e_r^I, it will bring about losing control of vehicles.

2.7 Crawler Robot

Crawler Robots, mainly used for inspecting pipelines [30], large ships or storage tanks, are another type of equipment in the remote visual inspection (RVI) technical kit. The operation of the crawler robot is very similar to that of a remote-control car with a controlled camera when lengthy distances must be travelled to do the check. Robotic lanes

require a long control distance and long battery life. Most robotic lanes come with tank pedals or miniature construction tires, as foreign debris is a real threat to mobility [31].describes the mathematical model of the suspension of robot traction of crawler type shown in [32]. in the mentioned model, to reduce mechanical vibrations caused by the operation of the motors and overcome obstacles in a path.

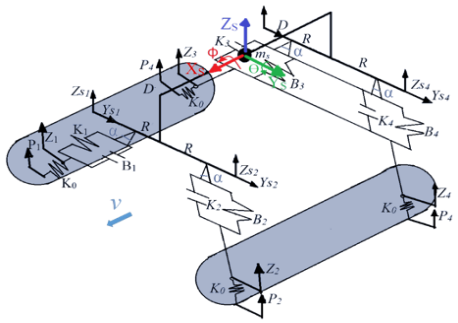

Figure 8. The traction crawler Scheme parametric [19]

To investigate the robot's dynamic behaviour, a reference system located at its centre of gravity which is used to determine the relative positions of the points of interest, Then, the lateral displacement is analyzed Y, and the vertical displacement Z. Additionally, is represented the angular displacement in the axes X and Y, which result in the roll and pitch angle respectively. The following parametric scheme (Fig. X) of the robot represents a model 12 degrees of freedom because of the displacement in Z and Y, of each of the reference points of the rigid body m_s, like contemplating the pitch angles θ and roll ϕ.For analysis Z one considers each reference point (1-4) (see Fig. 9), taking into account the inclination angle produced by the opening of the rubber tracks, the forces of the system are obtained.

$$\begin{aligned} FKz &= FK\cos\ \alpha \\ FBz &= FB\cos\ \alpha \\ FK_0z &= FK_0\cos\ \alpha \end{aligned} \quad (147)$$

The following equation represents the input signal.

$$P_{i_{1-4}}z = P_{i_{1-4}}\cos\ \alpha \quad (148)$$

$$\begin{aligned} \sum F &= m_oZ_{i_{1-4}}{}^* \\ FKz + FBz - FK_0 - W &= m_oZ_{i_{1-4}} \end{aligned} \quad (149)$$

The following equations represent the forces acting on the sprung mass.Forces acting on the left side:

$$FIz = FK_1z + FB_1z + FK_3z + FB_3z \quad (150)$$

Forces acting on the right side:

$$\begin{aligned} FDz &= F_2z + F_4z \\ FDz &= FK_2z + FB_2z + FK_4z + FB_4z \end{aligned} \quad (151)$$

$$\begin{aligned} \sum Fz &= m_sZ_s''(t) \\ -FIz - FDz - m_sg &= m_sZ_s''(t) \end{aligned} \quad (152)$$

For analysis at Y is followed a similar process than Z.

$$\begin{aligned} FKy &= FK\text{sen}\ \alpha \\ FBy &= FB\text{sen}\ \alpha \\ FK_0y &= FK_0\text{sen}\ \alpha \\ P_{i_{1-4}}y &= P_{i_{1-4}}\ \text{sen\alpha} \end{aligned} \quad (153)$$

Mathematical Analysis in Y for reference points $(1-4)$:

$$FKz + FBz - FK_0 - W = m_0Y_{i_{1-4}}{}' \quad (154)$$

Mathematical analysis regarding the lateral axis Y (sprung mass).Forces acting on the left side:

$$FIy = F_1y + F_3y \quad (155)$$

Forces acting on the right side:

$$FDy = F_2y + F_4y \quad (156)$$

Is obtained the equation of the sprung mass.

$$-FIy + FDy = m_sY_s(t) \quad (157)$$

Mathematical analysis regarding the angles of rotation (pitch and roll). Only the rotation angles produced by overpassing obstacles is studied because $v \approx 90$ mm/s Analysis Pitch: I_θ is the moment of inertia generated about axis Y (Fig. X).

$$\begin{aligned} I_\theta\ddot{\theta} &= (F_1z)D_f + (F_2z)D_f - (F_3z)D_r - (F_4z)D_r \\ &-(F_1y)D_f + (F_2y)D_f + (F_3y)D_r - (F_4y)D_r \end{aligned} \quad (158)$$

$$Ys_1 = Y_s + D_f\theta \quad (159)$$

$$\begin{aligned} Ys_2 &= Y_s + D_f\theta \\ Ys_3 &= Y_s - D_r\theta \\ Ys_4 &= Y_s - D_r\theta \end{aligned} \quad (160)$$

Analysis Roll: I_ϕ is the moment of inertia generated about axis X (Fig. X).

$$I_\phi\ddot{\phi} = (F_1z)R_f - (F_2z)R_f + (F_3z)R_r - (F_4z)H_r \quad (161)$$

2.8 Legged Robot

Legged robots are mobile robots that use mechanical limbs to move, like wheeled robots, but move more complexly than wheeled robots, which perform better than wheeled robots on rough terrain and are essential in most applications, such as one-legged robots: two-Legged

Robot, Three-Legged Robot, Four-Legged Robot, Six-Legged Robot and Multi-Legged Robot [33]. The model presented in [34] a complete kinematical model and dynamic model of a hexapod robot's leg. In order to obtain a more precise model we divided the mass of each link in two (M_i –servomotor mass, m_i-link mass, $M_i > m_i$).

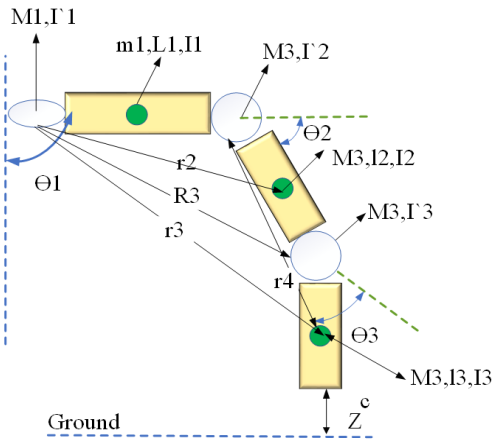

Figure 9. the legged robot Scheme

Considering the generalized coordinates vector $q = [q_1, q_2, q_3]^T$ the generalized vector forces can be computed using the below equation:

$$\tau_i = \frac{d}{dt}\left(\frac{\partial L}{\partial \dot{q}_i}\right) - \frac{\partial L}{\partial q_i} \tag{162}$$

where: $L(q, \dot{q}) = E_c(q, \dot{q}) - E_p(q)$

Considering that all three servomotors have the same mass $M_1 = M_2 = M_3 = M$ and the last two links have the same mass $m_2 = m_3 = m_2$ but different length the expressions for generalized forces are:

$$\begin{aligned}
&\tau_1 = \ddot{\theta}_1\left(I_1' + I_1'' + M(l_1^2 + R_3^2) + m_2(r_2^2 + r_3^2)\right)\\
&\tau_2 = \ddot{\theta}_2(I_2' + I_2'' + Ml_2^2 + m_3 r_4^2) - \{g[l_3\cos(\theta_2 + \theta_3) *\\
&\left(3M + m_1 + \frac{3m_2}{2}\right) + l_2\cos(\theta_2)\left(2M + m_1 + \frac{m_2}{2}\right)]\}\\
&\tau_3 = \ddot{\theta}_3(I_3' + I_3'') - gl_3\cos(\theta_2 + \theta_3)\left(3M + m_1 + \frac{3m_2}{2}\right)
\end{aligned} \tag{163}$$

where I_i' are the moments of inertia associated with the servomotors;I_i'' are the moments of inertia associated with the links;r_i radius of the instantaneous circle of rotation of the center of mass associated with the link i of the leg($i = 2 \ldots 4$);R_3 radius of the instantaneous circle of rotation of the servomotor 3 . The other Mathematical model for this type of biped robot leg with three links and four degrees of freedom was modelled using DH convention and Lagrange Euler equation[35].

$$A_i^{-1} = \begin{bmatrix} \cos(\theta_i) & -\sin(\theta_i)\cos(\alpha_t) & \sin(\theta_i)\sin(\alpha_i) & a\cos(\theta_i) \\ \sin(\theta_i) & \cos(\theta_i)\cos(\alpha_i) & -\cos(\theta_i)\sin(\alpha_i) & a\sin(\theta_i) \\ 0 & \sin(\alpha_i) & \cos(\alpha_i) & d_i \\ 0 & 0 & 0 & 1 \end{bmatrix} \tag{164}$$

Using the Lagrange-Euler equations, the following equation is derived by utilizing the kinetic and potential energy of every link in the system as given:

$$\frac{d}{dt}\frac{\partial K}{\partial \dot{q}} - \frac{\partial K}{\partial q} + \frac{\partial P}{\partial q} = Q \tag{165}$$

Where K and P represent kinetic and potential energy, respectively and Q is a vector with non-conservative forces like damping, applied torques and various kinds of friction. Kinetic energy is the amount of energy that a system has. Using the following formulas, we can determine Kinetic and Potential energy for the entire system:

$$K = \frac{1}{2}q^T\left(\sum_{i=1}^n m_i J_{vi}{}^T J_{vi} + J_{wi}^T R_i I_i R_i^T J_{wi}\right)\dot{q} \tag{166}$$

We can simplify it as follow:

$$D = \left(\sum_{i=1}^n m_i J_{vi}{}^T J_{vi} + J_{wi}^T R_i I_i R_i^T J_{wi}\right) \tag{167}$$

In equation (167) D is called the inertia matrix. The potential energy of a system with links i in a gravity field g with its centre of mass at the position for each link O_{ci} is:

$$P = \sum_{i=1}^n m_i g^T o_{ci} \tag{168}$$

The equations of motion can be derived using the Lagrange Euler equation, but we can simplify the process by assuming that no external forces are operating on the system other than the applied torques, which can be rewritten as in equation (169):

$$\frac{d}{dt}\frac{\partial L}{\partial q_i} - \frac{\partial L}{\partial q_i} = \Gamma_i \tag{169}$$

Where $L = K - P$ and q_i and Γ_i are the link I joint variable and joint torque Assume that the joint has no damping or friction, and that Q merely contains joint torques. For each link I the Lagrange-Euler equations are as follows:

$$\sum_{j=1}^n d_{ij}\ddot{q}_j + \sum_{k=1}^n \sum_{j=1}^n \left(\frac{d_{ij}}{\partial q_k} - \frac{1}{2}\frac{\partial d_{kj}}{\partial q_i}\right)\dot{q}_k\dot{q}_j + \frac{\partial P}{\partial q_i} = \Gamma_i(3.7) \tag{170}$$

This in matrix form can be written as:

$$D\ddot{q} + C\dot{q} + G = \Gamma \tag{171}$$

Where D is inertia matrix, C is coriolis and centrifugal matrix and G is gravity vector. The final set point θ_f is calculated as:

$$\theta_f = \begin{bmatrix} \theta_{1z} \\ \theta_{2z} \\ \theta_{3z} \\ \theta_{4z} \end{bmatrix} = \begin{matrix} 0 \\ 0 \\ 0 \\ \left[-\frac{\pi}{2}\right] \end{matrix} \tag{172}$$

The difference between the setpoint and the initial value of the joint angles that is denoted as θ_0 is represented as:

$$e(\theta_1) = \theta_{1z} - \theta_1 \quad (173)$$
$$e(\theta_2) = \theta_{2z} - \theta_2$$
$$e(\theta_3) = \theta_{3z} - \theta_3$$
$$e(\theta_4) = \theta_{4z} - \theta_4$$

Every system should ideally have an error signal that is set to zero so the initial position is:

$$\theta_0 = \begin{matrix} 0 \\ 0 \\ 0 \\ \left[\frac{\pi}{2}\right] \end{matrix} \quad (174)$$

In order to implement a PID controller on a system we need to give it the following equation:

$$\tau = K_P e + K_D \dot{e} + K_I \int e \quad (175)$$

We have four different inputs therefore the equation for each is:

$$\begin{aligned} \tau_1 &= K_p e(\theta_1) + K_D e(\theta_1) + K_1 \int e(\theta_1) \\ \tau_2 &= K_{P2} e(\theta_1) + K_{D2} e(\dot{\theta}_1) + K_{I2} \int e(\theta_2) \\ \tau_3 &= K_{P3} e(\theta_3) + K_{D3} e(\theta_3) + K_{I3} \int e(\theta_3) \\ \tau_4 &= K_{P4} e(\theta_4) + K_{D4} e(\dot{\theta}_4) + K_{14} \int e(\theta_4) \end{aligned} \quad (176)$$

In order to solve on Matlab and to understand the programming, the following equations as system equations can be used :

$$\begin{aligned} x_1 &= \theta_{1z} - \theta_1 \\ \dot{x}_2 &= \theta_{2z} - \theta_2 \\ \dot{x}_3 &= \theta_{3z} - \theta_3 \\ \dot{x}_4 &= \theta_{4z} - \theta_4 \end{aligned} \quad (177)$$

The characteristics of the two controllers were tweaked to have the optimal performance by trial and error. The following were found to be the optimal settings for the parameters:

$$\begin{aligned} \mathrm{K_{PID1}} &= \begin{bmatrix} K_{P1} \\ K_{D1} \\ K_{I1} \end{bmatrix} = \begin{bmatrix} 15 \\ 3 \\ 2 \end{bmatrix} \\ \mathrm{K_{PID2}} &= \begin{bmatrix} K_{P2} \\ K_{D2} \\ K_{I2} \end{bmatrix} = \begin{bmatrix} 15 \\ 4 \\ 2 \end{bmatrix} \\ \mathrm{K_{PID3}} &= \begin{bmatrix} K_{P3} \\ K_{D3} \\ K_{I3} \end{bmatrix} = \begin{bmatrix} 20 \\ 5 \\ 4 \end{bmatrix} \\ \mathrm{K_{PID4}} &= \begin{bmatrix} K_{P4} \\ K_{D4} \\ K_{I4} \end{bmatrix} = \begin{bmatrix} 10 \\ 5 \\ 5 \end{bmatrix} \end{aligned} \quad (178)$$

Observing the structure of the preceding ODE with control, we can see that (roughly): K_P is related to direct error and evolution speed.The pace of interaction with changes in states is connected to K_D.Overall error cancellation is connected to K_I

2.9 Snake Robot

Snake Robot is a new type of robot known as the Serpentine Robot. As the name suggests, these robots have multiple drive joints and, therefore, multiple degrees of freedom. This allows them to take advantage of Infinite's vast configuration, adapt, touch, and come close to a large capacity in their workspace [36].The omni-tread snake robot [37], Caleb III, presented in [38] designed to locomote on narrow space and rough terrain. Caleb III consists of three parts linked together by 2 DOF joints for pitch and yaw movements. The four sides of each segment have movable orbits that provide propulsion even when the robot is rolling. 2 D.O.F. connectors are actuated by 2 servomotors that produce sufficient torque to lift a front or next segment overcome obstacles.

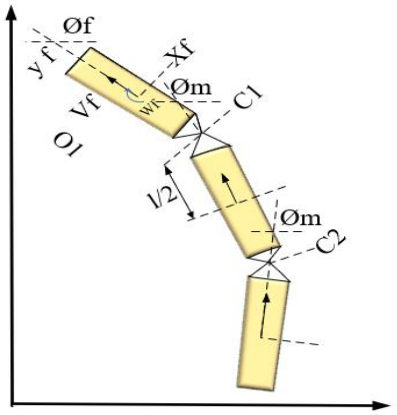

Figure 7. Snake Robot Schematic

Figure 10 shows the schematic of the snake where Caleb III has articulated steering as shown and the motion of the robot is analyzed by representative points in the front frame, middle frame and rear frame. Then the following equation is obtained:

$$\theta_f - \theta_m = \phi_1 \quad (179)$$
$$\theta_m - \theta_r = \phi_2$$

Here ϕ_1, ϕ_2 is the steering angle. Eqs. 172 is rewritten as follows by using the angular velocity ω_f, ω_m and ω_r of the front, middle and rear frame:

$$\omega_f - \omega_m = \frac{d\phi_1}{dt} \quad (181)$$
$$\omega_m - \omega_r = \frac{d\phi_2}{dt}$$

The velocity vector of the front, middle and rear frame ${}^f v_f$, ${}^m v_m$ and ${}^r v_r$ are expressed as follows based on the assumption of no-slip in the lateral direction:

$$
\begin{aligned}
{}^{f}v_f &= [v_f \quad 0]^r \\
{}^{m}v_m &= [v_m \quad 0]^T \\
{}^{r}v_r &= [v_r \quad 0]^T
\end{aligned}
\tag{182}
$$

The velocity vector $\left(s_{v_q}\right)$ of the first joint C_1 relative to the front frame is expressed as follows:

$$
{}_{v}v_{c_1} = \left[v_f \quad -\frac{L}{2}\omega_f\right]^T \tag{183}
$$

The velocity vector $\left(m_{c_1}\right)$ of the first joint C_1 relative to the middle frame is expressed as follows:

$$
{}^{m}v_{c_1} = \left[v_m \quad \frac{L}{2}\omega_m\right]^T \tag{184}
$$

The velocity vector $\left({}^{m}v_{c_2}\right)$ of the second joint C_2 relative to the middle frame is expressed as follows:

$$
m_{c_2} = \left[v_m \quad -\frac{L}{2}\omega_m\right]^T \tag{185}
$$

The velocity vector $\left(r_{c_2}\right)$ of the second joint C_2 relative to the rear frame is expressed as follows:

$$
rv_{c_2} = \left[v_r \quad \frac{L}{2}\omega_r\right]^T \tag{186}
$$

Since ${}_{v}v_q$ and m_q have to be the same, also ${}^{m}v_{c_2}$ and r_{v_a} have to be the same, the following equations are obtained:

$$
\begin{aligned}
\begin{bmatrix} v_f \\ -\omega_f \frac{L}{2} \end{bmatrix} &= \begin{bmatrix} \cos\phi_1 & \sin\phi_1 \\ -\sin\phi_1 & \cos\phi_1 \end{bmatrix} \begin{bmatrix} v_m \\ \omega_m \frac{L}{2} \end{bmatrix} \\
\begin{bmatrix} v_m \\ -\omega_m \frac{L}{2} \end{bmatrix} &= \begin{bmatrix} \cos\phi_2 & \sin\phi_2 \\ -\sin\phi_2 & \cos\phi_2 \end{bmatrix} \begin{bmatrix} v_r \\ \omega_r \frac{L}{2} \end{bmatrix}
\end{aligned}
\tag{186}
$$

From Eqs. (187) the next equations are obtained.

$$
\begin{aligned}
\omega_f &= \frac{1}{1+\cos\phi_1}\frac{d\phi_1}{dt} + \frac{2}{L}\tan\left(\frac{\phi_1}{2}\right)v_f \\
v_f &= v_m - \frac{L}{2}\tan\left(\frac{\phi_1}{2}\right)\frac{d\phi_1}{dt} \\
v_m &= v_r - \frac{L}{2}\tan\left(\frac{\phi_2}{2}\right)\frac{d\phi_2}{dt}
\end{aligned}
\tag{187}
$$

These Equations indicate the kinematic restrain conditions of the Caleb III. The position (x, y) and orientation θ_f of the front body at the base frame $\sum_w$ are expressed as follows:

$$
\begin{aligned}
x_f(t) &= x_{f0} + \int v_f(t)\cos\theta_f(t)dt \\
y_f(t) &= y_{f0} + \int v_f(t)\sin\theta_f(t)dt \\
\theta_f(t) &= \theta_{f0} + \int w_f(t)dt
\end{aligned}
\tag{188}
$$

Here, $x_{f0}y_{f0}$ and θ_{f0} are initial value. The other shape of this robot type, known as the worm robot prototype, is presented in [39-41] as shown in figure 11.

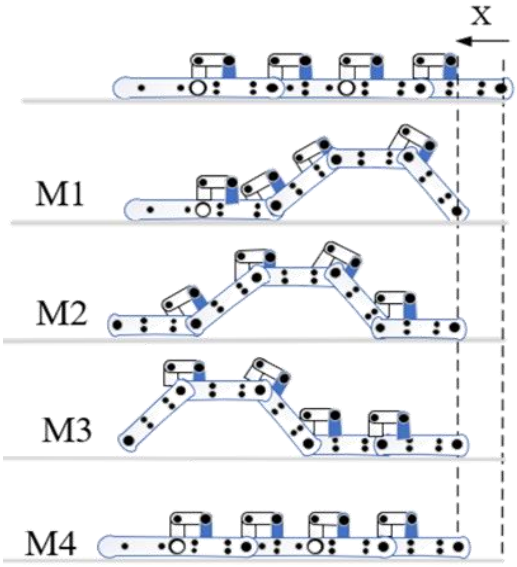

Figure 8. Snake Robot Schematic [25].

To assess the torque required in the Sub-Motion, it is necessary to solve the inverse dynamic problem as a function of the given nominal path. Therefore, the dynamic equations which govern each sub-motion must be available. The equations of motion in each sub-motion are established using a set of local coordinates. Therefore, we present the following local coordinate sets, which relate to the global coordinate set shown in Figure 11.

$$
\begin{aligned}
\{\theta_1, \theta_2, \theta_3\}^t &:= \{\theta_2^*, \theta_3^*, \theta_4^*\}^t \quad \text{in sub-motion } M_1 \\
\{\theta_1, \theta_2, \theta_3, \theta_4\}^t &:= \{\theta_1^*, \theta_2^*, \theta_3^*, \theta_4^*\}^t \quad \text{in sub-motion } M_2
\end{aligned}
\tag{182}
$$

Since the use of equations of motion is aimed at solving inverse dynamic problems rather than controlling, and interpretation is made based on the absolute angle of the connecting rod (measured in a positive direction with respect to the horizontal axis) and is calculated as follows:

$$
\varphi_0 = 0,\ \varphi_i = \varphi_{i-1} + \theta_i,\ i = 1, \ldots, n \tag{183}
$$

Also, the closed loop constraint in each sub-motion can be formulated as the below:

$$
\sum_{i=1}^{n} \sin\varphi_i = 0 \tag{189}
$$

Thus, the equations of motion governing in sub-motion M_1 has been explained as follows:

$$\frac{ml^2}{6}\begin{pmatrix}14 & 9 & c_{12} & 3 & c_{13}\\ 9 & c_{12} & 8 & 3 & c_{23}\\ 3 & c_{13} & 3 & c_{23} & 2\end{pmatrix}\begin{pmatrix}\ddot{\varphi}_1\\ \ddot{\varphi}_2\\ \ddot{\varphi}_3\end{pmatrix} + \frac{ml^2}{6}\begin{pmatrix}0 & 9 & s_{12} & & 3s_{13}\\ -9 & s_{12} & 0 & 3 & s_{23}\\ -3 & s_{13} & -3 & s_{23} & 0\end{pmatrix}\begin{pmatrix}\dot{\varphi}_1^2\\ \dot{\varphi}_2^2\\ \dot{\varphi}_3^2\end{pmatrix} + \frac{mgl}{2}\begin{pmatrix}5\cos\varphi_1\\ 3\cos\varphi_2\\ \cos\varphi_3\end{pmatrix} = \begin{pmatrix}1 & -1\\ 0 & 1\\ 0 & 0\end{pmatrix}\begin{pmatrix}\tau_1\\ \tau_2\end{pmatrix} + \begin{pmatrix}\lambda_1\\ \lambda_2\\ \lambda_3\end{pmatrix} \quad (190)$$

where, m and l denote the mass and length of the links, g is gravity acceleration, and for the sake of abbreviation it's taken $c_{ij} = \cos(\varphi_i - \varphi_j)$ and $s_{ij} = \sin(\varphi_i - \varphi_j)$. Similarly, in sub-motion M_2 the equations of motion are

$$ml^2\begin{pmatrix}20 & 15c_{12} & 9 & c_{13} & 3 & & c_{14}\\ 15 & c_{12} & 14 & 9 & c_{23} & 3 & c_{24}\\ 9 & c_{13} & 9 & c_{23} & 8 & 3 & c_{34}\\ 3 & c_{14} & 3 & c_{24} & 3 & c_{34} & 2\end{pmatrix}\begin{pmatrix}\ddot{\varphi}_1\\ \ddot{\varphi}_2\\ \ddot{\varphi}_3\\ \ddot{\varphi}_4\end{pmatrix} + \frac{ml^2}{6}\begin{pmatrix}0 & 15s_{12} & 9s_{13} & & & 3s_{14}\\ -15 & s_{12} & 0 & 9 & s_{23} & 3s_{24}\\ -9 & s_{13} & -9 & s_{23} & 0 & 3s_{34}\\ -3s_{14} & -3 & s_{24} & -3 & s_{34} & 0\end{pmatrix}\begin{pmatrix}\dot{\varphi}_1^2\\ \dot{\varphi}_2^2\\ \dot{\varphi}_3^2\\ \dot{\varphi}_4^2\end{pmatrix} \quad (191)$$
$$+\frac{mgl}{2}\begin{pmatrix}7cos\,\varphi_1 & 0 & & 0\\ 5 & & cos\,\varphi_2 & \\ 3cos\,\varphi_3 & 0 & 1 & -1\\ cos\,\varphi_4 & 0 & 0 & 1\\ 0 & 0 & & 0\end{pmatrix}\begin{pmatrix}\tau_1\\ \tau_2\\ \tau_3\end{pmatrix} + \begin{pmatrix}\lambda_2\\ \lambda_3\\ \lambda_4\end{pmatrix}R$$

Assuming a Coulomb friction model and using the Lagrange multiplier method, considering the stress equation, the normal component of the reaction, i.e. R, calculations can be performed from of the last row of the matrix form equation (191) given for the sub-motions M1 and M2 respectively, where we need to be replaced by:

$$\lambda_i = l_i(\cos\phi_i + \mu sgn(v_{tip}\cdot\hat{x})\sin\phi_i) \quad (192)$$

where, μ is the kinetic friction coefficient, and $\mathbf{v}_{tip}$ is the velocity vector of the tip of the last link in each sub-motion scuffing on the ground.

3. Conclusions

In the recent past, Automated Guided Vehicles (AGVs) have been the subject of a research effort to improve vehicle intelligence in different applications. Path tracking has been seen as a major challenge in autonomous mobile systems. Currently, some researchers are studying this problem under uncertain conditions such as dynamic obstacles and some known environments. This paper reviewed the different mathematical models for various AGV and service robots. Comparing the different AGV structures shows that the robot platform is mostly categorized based on its wheels or motion mechanism. To summarize, the AGV can be categorized as Differential type with Four, Six and Caterpillar, Independent's type, Ackerman, Legs and other structures as shown in figure (12). The following figure shows the types of service robots whose dynamic models are accumulated in this paper.

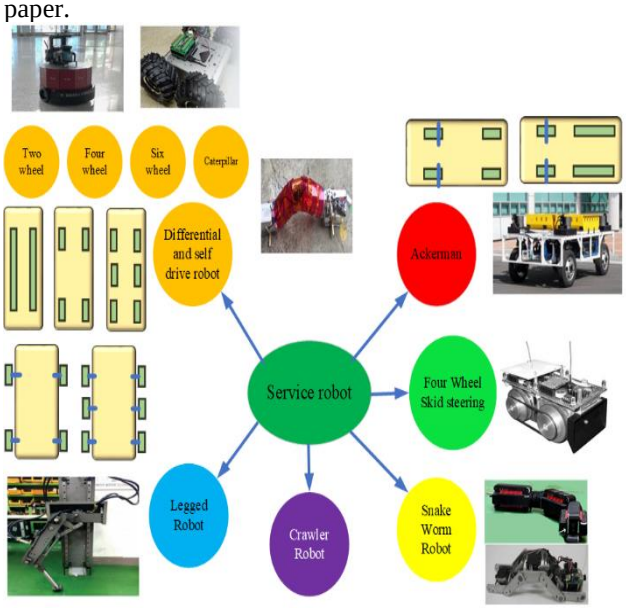

Figure 9. Types of service robot surveyed

based on the robots structures, the two Four- and six-wheel robots are typically used to carry higher payloads and / or to traverse rough terrain and they can offer good mobility. Compared to the four-wheel robot, the six-wheel robot has more redundancy in the event of wheel failure or loss. For the same tire size and vehicle mass, six wheels will exert less ground pressure than four wheels. However, six-wheeled vehicles of the same size may be heavier. Six wheels require more complex steering, drivetrain and suspension arrangements than four. To apply the same tractive force, the friction between the six-wheel drive and the ground is less than that of the four-wheel drive [42]. The applications of robotic could be extended on various potential works such as environmental, energy, hybrid materials, biomaterials, etc [43-52].

Acknowledgements.

- This work was supported by Jiangxi University of Science and Technology,341000, Ganzhou, P.R China, underfunding number: 205200100460.
- Authors thanking for their English proof reading

References

[1] A. J. Moshayedi, L. Jinsong, and L. Liao, "AGV (automated guided vehicle) robot: Mission and obstacles in design and performance," J. Simul. Anal. Nov. Technol. Mech. Eng., vol. 12, no. 4, pp. 5–18, 2019

[2] A. Jahangir Moshayedi, G. Xu, L. Liao, and A. Kolahdooz, “Gentle Survey on MIR Industrial Service Robots: Review & Design,” J. Mod. Process. Manuf. Prod., vol. 10, no. 1, pp. 31–50, 2021.

[3] A. J. Moshayedi, J. Li and L. Liao, "Simulation study and PID Tune of Automated Guided Vehicles (AGV)," 2021 IEEE International Conference on Computational Intelligence and Virtual Environments for Measurement Systems and Applications (CIVEMSA), Jun.2021, pp. 1-7, doi: 10.1109/CIVEMSA52099.2021.9493679.

[4] A. J. Moshayedi, “The quadrotor dynamic modeling and study of meta-heuristic algorithms performance on optimization of PID controller index to control angles and tracking the route The quadrotor dynamic modeling and study of meta-heuristic algorithms performance on optimiz,” no. September, 2020, doi: 10.11591/ijra.v9i4.pp256-270.

[5] A. Hemami, M. G. Mehrabi, and R. M. H. Cheng, “A New Control Strategy for Tracking in Mobile Robots and AGV’s.”

[6] J. Yi, H. Wang, J. Zhang, D. Song, S. Jayasuriya, and J. Liu, “Kinematic modeling and analysis of skid-steered mobile robots with applications to low-cost inertial-measurement-unit-based motion estimation,” IEEE transactions on robotics, vol. 25, no. 5, pp. 1087–1097, 2009.

[7] C. Jung and W. Chung, “Accurate calibration of two wheel differential mobile robots by using experimental heading errors,” in 2012 IEEE International Conference on Robotics and Automation, 2012, pp. 4533–4538.

[8] A. J. Moshayedi, J. Li, and L. Liao, “Simulation study and PID Tune of Automated Guided Vehicles (AGV),” in 2021 IEEE International Conference on Computational Intelligence and Virtual Environments for Measurement Systems and Applications (CIVEMSA), 2021, pp. 1–7.

[9] A. J. Moshayedi and D. C. Gharpure, “Evaluation of bio inspired Mokhtar: Odor localization system,” 2017, doi: 10.1109/CarpathianCC.2017.7970457

[10] O. Ringdahl, “Path Tracking and Obstacle Avoidance for Forest Machines,” Master's Thesis Umeå University Umeå, Sweden 2003 238 25.no. UMNAD 454/03, p. 72, 2003.

[11] A. J. Moshayedi and D. C. Gharpure, “Development of Position Monitoring system for studying performance of wind tracking algorithms,” in Robotics; Proceedings of ROBOTIK 2012; 7th German Conference on, 2012, pp. 1–4.

[12] A. J. Moshayedi, A. Abbasi, L. Liao, and S. Li, “Path planning and trajectroy tracking of a mobile robot using bio-inspired optimization algorithms and PID control,” 2019 IEEE Int. Conf. Comput. Intell. Virtual Environ. Meas. Syst. Appl. CIVEMSA 2019 - Proc., pp. 1–8, 2019, doi: 10.1109/CIVEMSA45640.2019.9071596

[13] A. J. Moshayedi, D. C. Gharpure, and E. Science, “Development of Position Monitoring system for studying performance of wind tracking algorithms Robot platform (Mokhtar) Zig Zag , Spiral algorithms,” vol. 32, pp. 161–164, 2012.

[14] H. Zhao, C. Luo, Y. Xu, and J. Li, “Differential Steering Control for 6× 6 Wheel-drive Mobile Robot,” in 2021 26th International Conference on Automation and Computing (ICAC), 2021, pp. 1–6.

[15] A. Abbasi and A. J. Moshayedi, “Trajectory Tracking of Two-Wheeled Mobile Robots, Using LQR Optimal Control Method, Based On Computational Model of KHEPERA IV,” Journal of Simulation & Analysis of Novel Technologies in Mechanical Engineering, vol. 10, no. 3, 2017.

[16] J. Harušinec, A. Suchánek, M. Loulová, and P. Kurčík, “Design of a prototype frame of an electrically driven three-wheel vehicle,” MATEC Web Conf., vol. 254, p. 02014, 2019, doi: 10.1051/matecconf/201925402014.

[17] J. F. Archila and M. Becker, “Mathematical models and design of an AGV (Automated Guided Vehicle),” in 2013 IEEE 8th Conference on Industrial Electronics and Applications (ICIEA), 2013, pp. 1857–1862.

[18] “Robotic Crawler,” ViewTech. Dec. 25, 2021.

[19] L. E. Solaque, M. I. Jaramillo, J. E. Zamudio, and D. A. Patiño, “Dynamic model of the suspension of a crawler type robot,” in 2014 III International Congress of Engineering Mechatronics and Automation (CIIMA), 2014, pp. 1–5.

[20] “Legged robots features, types, uses, advantages and disadvantages | Science online.” Dec. 25, 2019.

[21] M. O. Sorin, N. Mircea, and V. Stoian, “Hexapod robot. Mathematical support for modeling and control,” in 15th International Conference on System Theory, Control and Computing, 2011, pp. 1–6.

[22] R. Gautam and A. T. Patil, “Modeling and control of joint angles of a biped robot leg using PID controllers,” in 2015 IEEE international conference on engineering and technology (ICETECH), 2015, pp. 1–5.

[23] K. Kozłowski and D. Pazderski, “Modeling and control of a 4-wheel skid-steering mobile robot,” International journal of applied mathematics and computer science, vol. 14, pp. 477–496, 2004.

[24] J. L. Martínez, A. Mandow, J. Morales, S. Pedraza, and A. Garcia-Cerezo, “Approximating kinematics for tracked mobile robots,” The International Journal of Robotics Research, vol. 24, no. 10, pp. 867–878, 2005.

[25] Robotshop.com. 2022. 4 & 6 Wheel Robots - RobotShop. [online] Available at: <https://www.robotshop.com/en/4-wheeled-development-platforms.html> [Accessed 18 February 2022

[26] C. Koch, K. Georgieva, V. Kasireddy, B. Akinci, and P. Fieguth, “A review on computer vision based defect detection and condition assessment of concrete and asphalt civil infrastructure,” Adv. Eng. Informatics, vol. 29, no. 2, pp. 196–210, 2015, doi: 10.1016/j.aei.2015.01.008.

[27] M. W. Choi, J. S. Park, B. S. Lee, and M. H. Lee, “The performance of independent wheels steering vehicle(4WS) applied Ackerman geometry,” 2008 Int. Conf. Control. Autom. Syst. ICCAS 2008, pp. 197–202, 2008, doi: 10.1109/ICCAS.2008.4694549.

[28] H. Surmann, A. Bredenfeld, T. Christaller, R. Frings, U. Petersen, and T. Wisspeintner, “The Volksbot,” Work. Proc. Int. Conf. Simulation, Model. Program. Auton. Robot., no. August 2014, pp. 551–561, 2008.

[29] Nevon Projects. 2022. Robotic vehicle using Ackermann Steering Mechanism. [online] Available at: <https://nevonprojects.com/robotic-vehicle-using-ackermann-steering-mechanism.> [Accessed 19 February 2022].

[30] X. Ren and Z. Cai, “Kinematics model of unmanned driving vehicle,” in 2010 8th World Congress on Intelligent Control and Automation, 2010, pp. 5910–5914.

[31] A. J. Moshayedi, A. S. Roy, and L. Liao, “PID Tuning Method on AGV(Automated Guided Vehicle) Industrial Robot,” vol. 12, no. 4, pp. 53–66, 2020

[32] H. Zhang and J. Zhang, “Yaw torque control of electric vehicle stability,” in 2012 IEEE 6th International Conference on Information and Automation for Sustainability, 2012, pp. 318–322.

[33] S. Azam, F. Munir, and M. Jeon, "Dynamic control system design for autonomous car," in VEHITS 2020 - Proceedings of the 6th International Conference on Vehicle Technology and Intelligent Transport Systems, 2020, pp. 456–463. doi: 10.5220/0009392904560463.

[34] J. Xu, J. Liu, J. Sheng, and J. Liu, "Arc path tracking algorithm of dual differential driving automated guided vehicle," in 2018 11th International Congress on Image and Signal Processing, BioMedical Engineering and Informatics (CISP-BMEI), 2018, pp. 1–7.

[35] D. Y. Qu and Y. Zhan, "Dynamics Model and Control of Path Following of Wheel Mobile Robot," in Key Engineering Materials, 2010, vol. 419, pp. 829–832.

[36] A. Topiwala, "Modeling and Simulation of a Differential Drive Mobile Robot," International Journal of Scientific & Engineering Research, vol. 7, p. 2016, 2016.

[37] Y. Liu and A. B. Farimani, "An Energy-Saving Snake Locomotion Gait Policy Using Deep Reinforcement Learning," 2021, [Online]. Available: http://arxiv.org/abs/2103.04511.

[38] S.-J. Oh, H.-J. Kwon, J. Lee, and H. Choi, "Mathematical modeling for omni-tread type snake robot," in 2007 International Conference on Control, Automation and Systems, 2007, pp. 1445–1449.

[39] S.-J. Oh, H.-J. Kwon, J. Lee, and H. Choi, "Mathematical modeling for omni-tread type snake robot," in 2007 International Conference on Control, Automation and Systems, 2007, pp. 1445–1449.

[40] M.-R. S. Noorani, A. Ghanbari, and S. Aghli, "Design and fabrication of a worm robot prototype," in 2015 3rd RSI International Conference on Robotics and Mechatronics (ICROM), 2015, pp. 73–78.

[41] A. J. Moshayedi, S. S. Fard, L. Liao, and S. A. Eftekhari, "Design and Development of Pipe Inspection Robot Meant for Resizable Pipe Lines," Int. J. Robot. Control, vol. 2, no. 1, p. 25, 2019, doi: 10.5430/ijrc.v2n1p25.

[42] F. Ju, W. Zhuang, L. Wang, and Z. Zhang, "Comparison of four-wheel-drive hybrid powertrain configurations," Energy, vol. 209, p. 118286, 2020, doi: https://doi.org/10.1016/j.energy.2020.118286.

[43] S. Tian, N. I. Arshad, D. Toghraie, S. A. Eftekhari, and M. Hekmatifar, "Using perceptron feed-forward Artificial Neural Network (ANN) for predicting the thermal conductivity of graphene oxide-Al2O3/water-ethylene glycol hybrid nanofluid," Case Stud. Therm. Eng., vol. 26, p. 101055, 2021.

[44] Hojjati Najafabadi, A., A. Ghasemi, and R. Mozaffarinia, Development of novel magnetic-dielectric ceramics for enhancement of reflection loss in X band. Ceramics International, 2016. 42(12): p. 13625-13634.

[45] H. Amirabadi, F. Farhatnia, S. A. Eftekhari, and R. Hosseini-Ara, "Free vibration analysis of rotating functionally graded GPL-reinforced truncated thick conical shells under different boundary conditions," Mech. Based Des. Struct. Mach., pp. 1–32, Sep. 2020, doi: 10.1080/15397734.2020.1822183.

[46] Torkian, N., et al., Synthesis and characterization of Ag-ion-exchanged zeolite/TiO2 nanocomposites for antibacterial applications and photocatalytic degradation of antibiotics. Environmental Research, 2022. 207: p. 112157.

[47] Hojjati-Najafabadi, A., et al., Antibacterial and photocatalytic behaviour of green synthesis of Zn0.95Ag0.05O nanoparticles using herbal medicine extract. Ceramics International, 2021. 47(22): p. 31617-31624.

[48] Hojjati-Najafabadi, A., A. Ghasemi, and R. Mozaffarinia, Magneto-electric features of BaFe9.5Al1.5CrO19-CaCu3Ti4O12 nanocomposites. Ceramics International, 2017. 43(1, Part A): p. 244-249.

[49] Hojjati-Najafabadi, A., et al., A Tramadol Drug Electrochemical Sensor Amplified by Biosynthesized Au Nanoparticle Using Mentha aquatic Extract and Ionic Liquid. Topics in Catalysis, 2021.

[50] B. Liao, J. Li, S. Li, and Z. Li, "EAI Endorsed Transactions Briefly Revisit Kinematic Control of Redundant Manipulators via Constrained Optimization," pp. 1–7, doi: 10.4108/XX.X.X.XX.

[51] J. Peng, T. Wen, Y. Yang, and G. Huang, "on AI and Robotics EAI Endorsed Transactions An Event-B Approach to the Development of Fork / Join Parallel Programs," pp. 1–6, doi: 10.4108/XX.X.X.XX.

[52] A. J. Moshayedi, A. S. Roy, A. Kolahdooz, and Y. Shuxin, "EAI Endorsed Transactions Deep Learning Application Pros and Cons Over Algorithm," pp. 1–13, doi: 10.4108/XX.X.X.XX.